Energy Storage and Conversion 2025, 3(4), 3826.
doi: https://doi.org/10.59400/esc3826

Review

Ammonia synthesis and decomposition mediated by hydrides, imides, and amides

Muhammad Anis Aslam[1], Sajad Hussain[2], Ismat Ullah Khan[3,*]

[1] Shanghai Key Laboratory of Hydrogen Science & Centre of Hydrogen Science, School of Materials Science and Engineering, Shanghai Jiao Tong University, Shanghai 200240, China

[2] Department of Environmental Sciences, Comsats University Islamabad, Vehari Campus, Vehari 61100, Pakistan

[3] Department of Chemistry, Government Post Graduate College (GPGC), Lakki Marwat 28420, Pakistan

*** Corresponding author:** Ismat Ullah Khan, iukhan@chem.qau.edu.pk

CITATION

Aslam MA, Hussain S, Khan IU. Ammonia synthesis and decomposition mediated by hydrides, imides, and amides. Energy Storage and Conversion. 2025; 3(4): 3826. https://doi.org/10.59400/esc3826

ARTICLE INFO

Received: 3 August 2025
Revised: 7 September 2025
Accepted: 11 September 2025
Available online: 5 October 2025

Abstract: Ammonia is used for global fertilizer production and is increasingly viewed as a viable carrier for renewable hydrogen and long-duration energy storage. Realizing this potential requires catalysts and process architectures that enable both N_2-to-NH_3 synthesis and NH_3-to-H_2 decomposition at substantially reduced temperature and pressure. This review surveys recent advances in which alkali- and alkaline-earth metal hydrides, amides, and imides act as dynamic redox and hydrogen/nitrogen-transfer media, undergoing reversible interconversion with N_2, H_2, and NH_3. We summarize thermocatalytic systems where hydridic H^- and electron-rich lattices promote N_2 activation, heterolytic H_2 cleavage, and N–H bond formation, including composite catalysts that exploit cooperative interfaces with transition metals and complex or mixed-anion hydrides that relax constraints imposed by conventional metal-only surfaces. We also discuss photo-assisted routes that leverage defect-stabilized charge carriers in hydrides to drive nitrogen conversion under illumination, and chemical-looping strategies that decouple nitrogen fixation from hydrogenation (or hydrogen release) to tune thermodynamics and mitigate competitive adsorption. Across these platforms, recurring motifs include lattice-mediated hydride/proton shuttling, interfacial electron donation, and reversible nitride–imide–amide formation that can be engineered to balance activity, selectivity, and stability. Finally, we outline key barriers to practical deployment, air/moisture sensitivity, carrier volatility, phase segregation, and limited operando understanding and highlight design priorities for stabilizing reactive phases and integrating reactors compatible with renewable heat, photons, or electricity, thereby enabling scalable and decentralized ammonia and hydrogen technologies.

Keywords: ammonia synthesis; hydrogen production; hydrides; imides; amides

1. Introduction

The consequences of global warming witnessed in the past century have led to the need to design and develop clean and sustainable sources of energy [1, 2]. Renewable energy is by far one of the most imperative sustainable solutions to the reduction of the environmental damage that the vast use of fossil fuels has created. Nonetheless, intermittency and uncertainty of renewable energy and the geographical disparity between energy production and consumption centers are serious obstacles to power generation through these sources. Such a gap complicates the provision of energy needs in the world. Thus, to narrow these time and space gaps, a special supply-demand

management system should be developed [3]. Replacement of carbon-based fuel by hydrogen-based energy carriers can be done through the fact that hydrogen is a high-energy storer, and its gravimetric density of 120 MJ per kilogram is very high [4]. However, hydrogen is not an efficient long-range energy carrier because its volumetric energy density of 9.8 kJ/L at standard temperature and pressure (STP) is much less than that of gasoline (31.7 MJ/L) and methanol (15.8 MJ/L) [5, 6]. The carbon footprint should be mitigated by coming up with sustainable technologies that would utilize, or utilize rather indirectly, carbon-free energy carriers. Hydrogen production through sustainable means is a subject that has been receiving a lot of attention in the last few decades, and this has led to the introduction of new and more efficient processes of producing H_2 using various hydrogen-based resources [7–10]. Hydrogen, being the lightest gas, has a much lower liquefaction temperature (about −250 °C) than the rest and needs a significantly greater volume per unit mass. To overcome these challenges, hydrogen can be transported and stored safely by converting it to a different chemical, which is commonly referred to as an energy vector. It can then be applied on-site by decomposing thermally or endothermically reforming it to the desired form [11]. Other promising materials to store liquid hydrogen transportable are chemical hydrides, ammonia, methanol, methylcyclohexane, formic acid, and methanol. Methanol was one of the initial alternatives to be considered in making hydrogen locally, but as it emits CO_X, it cannot be used in car engines. In addition, some of the metal hydrides, including $NaAlH_4$, $Mg(BH_4)_2$, and $LiAlH_4$, have been investigated as carbon-neutral sources to recycle hydrogen but were incapable of meeting the demands of on-site, reversible hydrogen storage. In the same way, the metal amine salts and metal–organic frameworks (MOFs) have been studied in terms of sustainable hydrogen production. Nevertheless, such techniques are not as viable as commercial applications because of the low capacity of MOFs to store hydrogen, and the challenges of thermal manipulation of amine-containing systems (including ammonia production). The Haber-Bosch process is the most common method of producing industrial amounts of ammonia today, with N_2 and H_2 reacting at high temperature (350–500 °C) and pressure (15–35 MPa) in the presence of an iron-based catalyst to produce NH_3 [12–14]. This process is known to be energy-demanding, and its carbon footprint is high, with an estimated consumption of 1~2% of the worldwide energy input and an annual carbon dioxide emission of more than 670 million tons. The proportion of the energy input into the process converted to the chemical energy of the ammonia molecule is approximately 60%; the remainder of the energy is lost, primarily in the hydrogen production of natural gas, production of ammonia, and gas separation [15–17]. The dissociation of ammonia is an endothermic reaction and is accompanied by rising entropy, and theoretical equilibrium conversion is greater than 99% at 400 °C. Nevertheless, high conversion rates are typically attained at high temperatures exceeding 600 °C because of a large kinetic barrier. Thus, the creation of an efficient catalyst is an issue of burning importance, and Ni-based and Ru-based catalysts are under analysis to this day. Ammonia synthesis and decomposition [18–21] are shown in **Figure 1**.

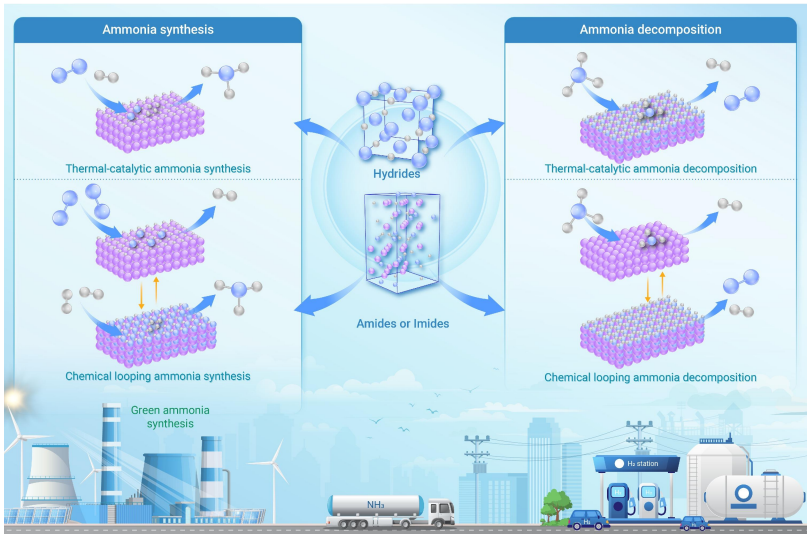

Figure 1. Roadmap: ammonia synthesis and decomposition were mediated by Hydrides, Imides, and Amides [22].

Recent work shows that alkali and alkaline-earth metal hydrides, amides, and imides can participate dynamically in nitrogen and hydrogen transformations. Their strongly reducing character, reversible interconversion among H- and N-containing phases, and cooperative behavior with transition metals enable alternative pathways for N_2 activation, N–H bond formation, and NH_3 decomposition, often under milder conditions than traditional metal catalysts. These materials also support chemical-looping concepts that separate nitrogen fixation from hydrogenation (or hydrogen release), reducing competitive adsorption and allowing thermodynamic tuning.

This review consolidates advances in thermocatalytic ammonia synthesis and cracking enabled by hydride/amide/imide chemistry, surveys photo-assisted routes that exploit long-lived charge carriers in hydrides, and evaluates chemical-looping strategies for both ammonia production and hydrogen generation. We highlight mechanistic insights, performance-limiting steps, and materials/reactor challenges—particularly air/moisture sensitivity, carrier volatility, phase segregation, and the need for operando understanding—to guide the design of robust, scalable systems compatible with renewable heat, photons, or electricity.

2. Ammonia as a hydrogen storage medium

Ammonia is a hydrogen storage and transportation medium that has a number of advantages. These are a large hydrogen storage capacity (17.7 wt.%), a comparatively simple liquefaction (at low temperatures, 0.86 MPa), a high volumetric energy density (108 kg H_2 m^{-3}), zero emissions of carbon, and the capability to generate the gas in large amounts by the well-established Haber-Bosch (HB) process. Still, the conventional HB process consumes a lot of energy and generates a lot of CO_2. Numerous methods of modernizing the existing technology have been suggested to make the synthesis of ammonia sustainable, with an emphasis on the use of water electrolysis to generate hydrogen [23,24]. The steam reforming of methanol or methane ($CH_4 + H_2O \rightleftharpoons CO + 3H_2$, with an enthalpy change of +68.7 kJ per mole of H_2) consumes more energy

compared to the decomposition of ammonia ($2NH_3 \rightleftharpoons N_2 + 3H_2$, with an enthalpy change of +30.6 kJ per mole of H_2). Therefore, ammonia decomposition is more economically feasible for on-site hydrogen regeneration [25]. The decomposition of ammonia in the production of H_2 has received significant attention, especially in the efforts to have a complete understanding of the reaction process. This is aimed at keeping the lowest practical reaction temperature and maximizing the conversion and hydrogen generation rate [26–29].

Thermodynamically, high conversion is achievable at 300 to 350 °C, ammonia can be broken down, and the conversion back to 96.0 to 98.0%. Nevertheless, the degradation of NH_3 catalyzed is normally at higher temperatures (above 450 °C) due to kinetic limitations. As a result, past researches have paid significant attention to the creation of catalysts that can decompose NH_3 at reduced temperatures [30–32]. Numerous strategies have been explored to lower the operating temperature of NH_3 decomposition, including tuning active-metal composition and particle size, optimizing supports, modifying reactor architectures, and engineering adsorption energetics. Reported intrinsic activity trends for NH_3 decomposition commonly place Ru among the most active metals; however, Ru catalysts can still show limited performance at ≤450 °C and are constrained by high cost. These limitations motivate the development of Ru-free alternatives, including Fe-, Ni-, and Co-based catalysts and bimetallic systems (e.g., CoMo, NiFe), often combined with high-surface-area supports (Al_2O_3, SiO_2, CaNH) and electronic promoters (K, Na, La, Ce) to improve activity and stability under practical conditions [33–42].

The comparison between ammonia and other common fuels is presented in detail in **Table 1**, but special attention is given to the energy density, heating values, and the volumetric and energetic costs [43]. Previous research has demonstrated that alkali metal hydrides and ammonia could offer a form of reversible hydrogen storage substance with a high capacity and the capability to liberate hydrogen under moderate conditions spontaneously. In this process, the reaction of desorption of hydrogen can be represented:

$$MH + NH_3 \rightarrow MNH_2 + H_2 (M = Li, K \text{ and } Na)$$

Table 1. Comparison between NH_3 and conventional fuels.

Type of fuel/storage	HHV ($MJkg^{-1}$)	Density (kgm^{-3})	Energy density (GJm^{-1})	P (MPa)	Specific energetic cost ($\$GJ^{-1}$)	Specific volumetric cost ($\$m^{-3}$)
H_2/metal hydrides	142	25	3.5	1.4	35.2	125
CNG (CH_4)/integrated storage system	55.5	188	10.4	25	38.3	400
Gasoline (C_8H_{28})/liquid tank	46.7	736	34.4	1	29.1	1000
Methanol	15.2	749	11.4	1	60.9	693
LPG	48.9	288	19	1.4	28.5	542
NH_3/metal amines	17.1	610	10.4	1	17.5	183
NH_3/pressurized tank	22.5	603	13.5	1	13.3	181

Note: HHV: Higher heating value, CNG: compressed natural gas, and LPG: liquefied petroleum gas.
Source: Reprinted with permission from the studies by Zamfirescu and Dincer [43] and Klerke et al. [44].

The key difficulty in creating hydrogen storage material using alkali metal hydrides and ammonia is to attain not only excellent kinetics of both hydrogenation and dehydrogenation taking place, but also a high storage capacity. The Li-NH_3 system contains the most hydrogen (8.1 wt.%) of the systems examined, and due to its exothermic hydrolysis-type reaction, it is possible to operate at relatively lower temperatures [45–48]. Li-NH_3 can also be improved with 5 mol.% of KH and KNH_2, which will enhance the kinetics of hydrogen desorption/absorption significantly. Attractive research is underway to study the catalytic properties of these compounds on the Li-NH_3 system, depending on potassium. Hydrogen desorption characteristics of the reactions between lithium hydride and NH_3 at temperatures of 50–200 °C in the presence of various particle sizes. The possibility of applying multiple potassium compounds to serve as catalysts to enhance the kinetics of the hydrogen desorption process of the Li-NH_3 system. In a study, it was revealed that three methods are efficient in enhancing the desorption kinetics of this system: doping by using potassium compounds, increasing the reaction temperature, and ball milling of the LiH particles to decrease their size [49]. As of late, new advancements in large-scale water electrolysis have provided significant promise in terms of the commercial generation of green hydrogen. A water electrolysis method should be sustainable, and to achieve this, power that is generated in a carbon-neutral environment, e.g., solar and wind energy, can be used. Then, in the cases where the commercial use is applicable, the nitrogen in the cryogenic air distilled mix and the green H_2 generated in the process could be combined to create carbon-free green ammonia. The NH_3 can then be cheaply distributed to all parts of the world and stored through the large capacity infrastructure that is now in existence. Finally, ammonia breakdown units that are located on-site could generate carbon-free, renewable H_2, which can be applicable in hydrogen refueling stations, fuel cells, internal combustion engines, or power generation systems. This discussion examines the prospects and challenges of the use of ammonia as an energy carrier and emphasizes the importance of hydrogen as a future fuel. It evaluates the methods of H_2 generation with the breakdown of NH_3 in different working conditions with reactor types and catalysts. The three major barriers to the establishment of a hydrogen-based economy of tomorrow are the creation of effective reactor systems, the advancement of H_2 purification technology, and the creation of cheap and efficient catalysts. At this point, there is a lot of research being conducted on the utilization of metal hydrides in ammonia synthesis and degradation. This research also has a comprehensive techno-economic analysis and operational feasibility study of a number of reactor designs. It gives recommendations to hasten the commercialization process, as per the literature, as well as our experience, to achieve maximum efficiency of the NH_3 breakdown and generation of green H_2. Considering the above, the creation of efficient catalysts and innovative processes of ammonia generation and breakdown under moderate conditions is urgent but extremely difficult for the development of the energy economy of ammonia-hydrogen. Indicatively, these recent reports have shown many types of new catalysts to ammonia synthesis, including electrodes supported metals (Ru/C12A7: e^- [50], Ru/Ca_2N: e^- [51,52], etc.), intermetallic compounds (LaCoSi [53], LaRuSi [54], etc.), rare earth metal nitrides or carbides supported transition metals

(LaN [55,56], CeN [57], CeC_2 [58], etc.). Moreover, since one of the centers of this review is hydrides, which contain hydride ions (H^-), strong reducing activities, and have a special role in the activation of nitrogen, they contain hydrogen [59]. At present, the hydrides mostly being utilized in the production of ammonia are: (i) binary metal hydrides (LiH [16], BaH_2 [60], TiH_2 [61] etc.), (ii) complex hydrides (Li_4RuH_6, Ba_2RuH_6, etc.) [62], (iii) mixed anion hydrides (Ln-OH [63], Sm_2O_3 (Sm-H) [64], $TiO_{2-x}H_y$ [65], Ba_5CrN_4H [66], $BaCeO_{3-x}N_yH$ [67], Hydride materials above, either (co)-catalysts or catalyst supportes in thermocatalytic ammonia production, alkali or alkaline earth metal hydrides (such as LiH, BaH_2) [68,69] as nitrogen carriers in chemical looping ammonia synthesis (CLAS) have been shown to perform well. The primary catalysts used in the breakdown of ammonia are (i) supported or non-supported monometallic catalysts (e.g., Fe, Co, Ni, Ru, Rh, Pt, Ir) [70–74]; (ii) supported or non-supported metal alloy catalysts (e.g., FeCo, CoNi) [75–78]; (iii), metal carbide catalysts (e.g., WC, MoC) [79]; (iv), metal nitride [2,6,25,80–87].

3. Thermocatalytic ammonia synthesis

3.1. Alkali and alkaline earth hydrides as catalysts

Ammonia synthesis, the opposite of ammonia breakdown, is a more significant process in catalysis and is regarded as a bellwether [61]. It is one of the reactions that has been most studied regarding heterogeneous catalysis. Over the previous century, the majority of periodic table elements have been sieved and judged on their catalytic ability in the rate of ammonia generation [88]. Fused iron and supported Ru catalysts have also been prepared in the case of the KAAP process and the Haber-Bosch process. There has been a well-established trend in volcanoes, which shows the extent to which the action of the ammonia synthesis process is sensitive to the nature of the transition metals. This pattern of activity has been successfully explained by the concept of energy scaling relations, i.e., the idea that the energies of the adsorption of reactive species on transition-metal surfaces scale with one another. Alloys or transition metals with small N adsorption energies, such as Fe, Ru, and CoMo, are useful catalysts in the synthesis of ammonia. Other transition metals do not because they will not bind N at all (strongly enough; Ni), or bind it too strongly (early 3d metals V, Cr, and Mn). A major challenge to the production of ammonia is the energy scaling relations [89,90].

3.2. Transition metals alkali hydride composite catalysts

The active for ammonia synthesis would make a suitable ammonia decomposition catalyst. We should naturally investigate the TM-Li_2NH combination for ammonia production. Higher H_2 partial pressure causes Li_2NH to convert to LiH, as shown in **Figure 2**. Therefore, in ammonia synthesis conditions, the TM-Li_2NH composite would change to TM-LiH. When early and late 3d transition metals from V to Ni come into contact with LiH, their kinetic behaviors and catalytic performances are dramatically changed [16]. **Figure 3a,b** illustrates how the addition of LiH at 573 K and WHSV of 600.000 mL g_{cat}^{-1} h^{-1} can increase ammonia synthesis rates by up to 3–4 orders of magnitude (except for Fe) when compared to bare TM(N). It has been

demonstrated that certain TMs, namely VN and CrN, as well as Ni, a late TM, are catalytically inactive; yet, they can catalyze the creation of ammonia at the proper rates when they combine with LiH. It's important to note that the Cr-, Mn-, Fe-, and Co-LiH catalysts have measurable activity at 423 K; at 523 and 573 K, they perform 12–20 and 2–3 times better, respectively, than the reference RuCs/MgO catalyst, as shown in **Figure 3c**.

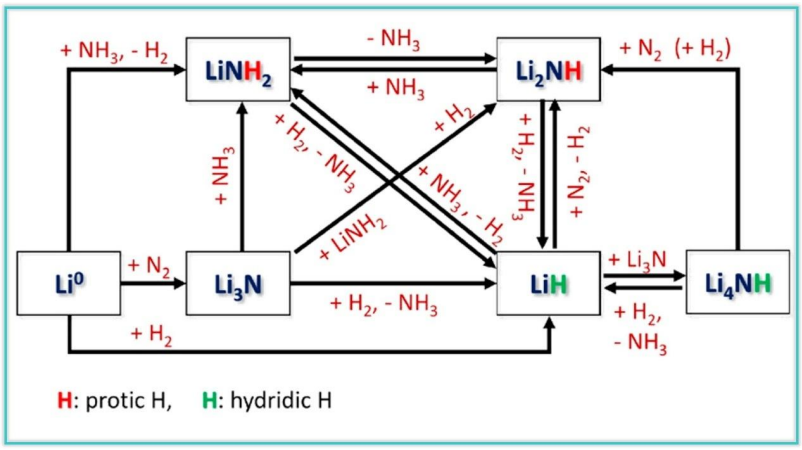

Figure 2. The lithium metal, hydride, nitride, amide, imide, and nitride-hydride interconvert [90].

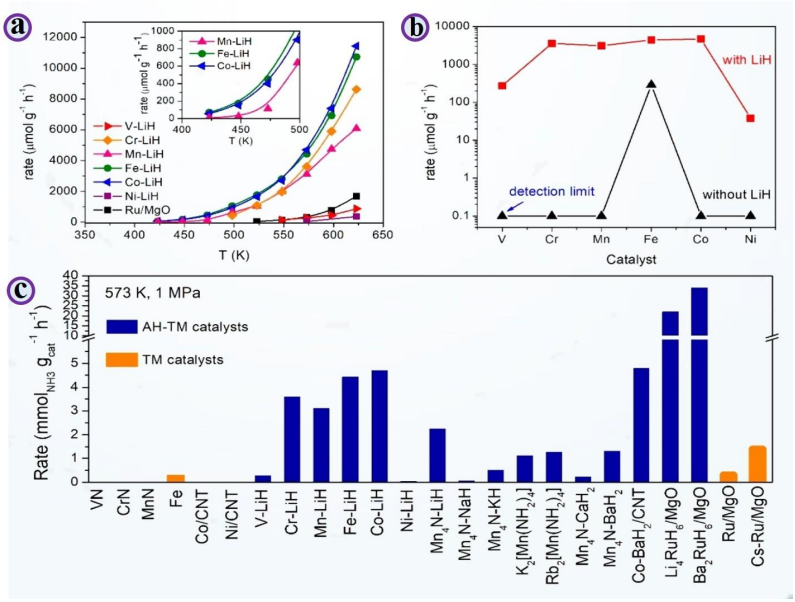

Figure 3. **(a)** Synthesis rate of ammonia of a series of TM-LiH catalysts versus temperature; The inset is the magnified version of the rates in the temperature range 420 to 500 K. N_2/H_2 = 1:3, pressure = 1 MPa; **(b)** activity of 3d TM (V to Ni) with or without LiH at 573 K and 1 MPa [16]; **(c)** Rates of ammonia synthesis regarding a sequence of alkali/alkaline earth hydroxide-containing catalysts and reference catalysts [22].

The most interesting experimental observation is the fact that, rather than the normal volcano-like behavior, the Cr-, Mn-, Fe-, and Co-LiH catalysts display similar activities and a high-land-like behavior (**Figure 3b**). This indicates that LiH enhances the catalytic activity of these TM(N) or causes an absence of catalysis depending on the binding energy of the transition metals to N. It is a clear indication that the

scaling relations of TM-only surfaces have been overused. Li was demonstrated to have the least promoting effect on transition metals in the synthesis of ammonia, with known ample promoting effects of the hydroxides of alkali or alkaline earth metals, in particular those of K, Cs, and Ba, on transition metals. The notable impact of LiH on TM is not typical. LiH is primarily distinguished from its (hydro)oxide counterparts by the existence of H–, an electron and proton carrier essential to its operation (i.e., H– in LiH may undergo reductive addition to form an N–H bond and weaken the N≡N triple bond). Additional research with other alkali and alkaline earth metal hydrides for ammonia catalysis highlights the significance of H^-. One way to increase the catalytic activity of Co metal is to combine it with barium hydride (BaH_2) [91]. The rate of ammonia synthesis of the Co-BaH_2 catalyzed by carbon nanotubes (CNTs) is around two orders of magnitude faster than the rate of BaO-Co/CNTs at 573 K and 1 MPa. On the same note, the catalytic activity of Mn nitride (e.g., Mn_4N) is enhanced one to three orders of magnitude by the presence of NaH, KH, CaH_2, or BaH_2. Mn nitride is mainly promoted in the AH order of BaH_2, LiH, KH, CaH_2, and NaH. This is not similar to conventional alkali or alkaline earth (hydra)oxide promoters [60]. **Figure 3c** shows the rates of ammonia synthesis of a series of TM-AH composite catalysts at different temperatures of 573 K and pressures of 1 MPa.

The linkage between transition metals, hydrogen, nitrogen, alkali/alkaline earth metals, and nitrogen is intuitive, and thus it is not surprising that hydride catalysts exhibit a great deal of increased activity. We proposed a two-active-center paradigm, which shows the synergy between the use of AHs and TM in catalyzing ammonia production. The rationale behind this model is the fact that separate TM and AH phases comprise the functional 3d TM-AH catalysts. This model entails three steps (**Figure 4a**) [16]. A useful framework is a dual-site mechanism in which adjacent transition-metal (TM) and alkali/alkaline-earth hydride (AH) phases cooperate. In this view, (i) N_2 is activated on TM sites, (ii) activated N species are transferred to the neighboring hydride phase, where hydridic H^- and electron density facilitate N–H bond formation, and (iii) subsequent hydrogenation steps proceed via heterolytic H_2 activation at the TM–AH interface, ultimately releasing NH_3 while regenerating reactive sites. This cooperative chemistry can mitigate limitations imposed by scaling relationships on TM-only surfaces, although key details—including interfacial structure, charge/proton (hydride) transfer pathways, and the dominant adsorption modes of N_2 and H_2—remain active topics of investigation.

Gas-phase cluster reaction experiments to provide profound mechanistic insights into the relationship between hydrides and transition metals. It has been suggested that structurally well-defined gas-phase clusters produced by a catalyst are appropriate models to match the catalyst's reactive site. Clusters formed from an Fe-LiH catalyst by laser ablation using gas-phase optical spectroscopy combined with mass spectrometry and quantum chemical computations [93, 94]. Several intricate hydride clusters, including $[LiNH2]^-$ [95] and $[Li_5FeH_6]^-$, were discovered. These hydride clusters changed into $[FeNH_2]^-$ and $[LiNH_2]^-$ moieties upon coming into contact with N_2, demonstrating the cleavage of the N≡N link as well as the production of N–H, Li–N, and Fe–N bonds (**Figure 4b**). While it is challenging to use traditional methods to

define the Fe-LiH catalyst's surface composition, the aforementioned cluster reactions suggest that [Li–Fe–H] species might be present and operate as the reactive site for N_2 activation and hydrogenation through an alternative mechanism. We speculated on the possibility that complex transition-metal hydrides could serve as effective catalysts for the synthesis of ammonia in light of these findings [92].

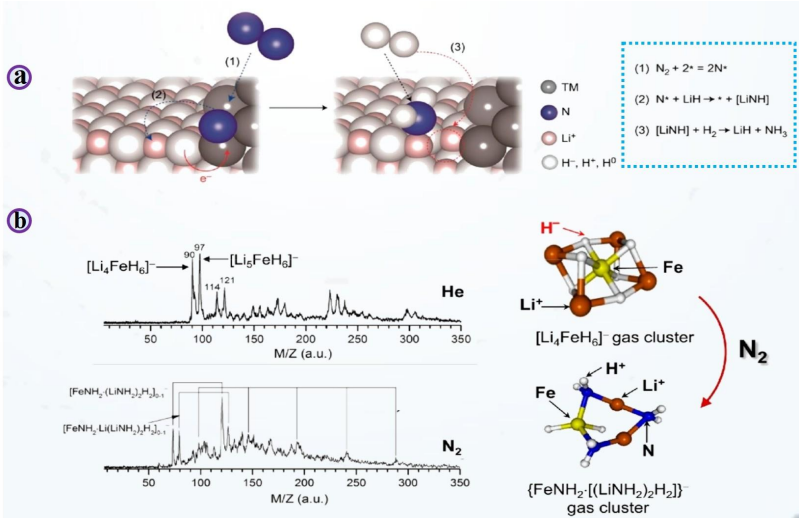

Figure 4. **(a)** Proposed reaction mechanism of ammonia synthesis catalyzed by TM-AH composite catalysts [16]; **(b)** Lithium iron hydride gas clusters react with N_2 to form [$LiNH_2$]-containing clusters [92].

3.3. Complex hydride catalysts

Although Li_4FeH_6 is known, it requires extreme synthesis conditions, whereas several ternary Ru hydrides (e.g., Li_4RuH_6 and Ba_2RuH_6) can be prepared under far milder conditions. These materials provide a practical testbed for the concept that complex hydrides can function as catalytic platforms for ammonia synthesis. Reported activity data show that Ba_2RuH_6 (often used with MgO) is among the most active catalysts under comparatively mild conditions; for example, at 573 K, its NH_3 synthesis rate exceeds that of conventional Cs–Ru/MgO, and ppm-level effluent NH_3 has been detected near ambient pressure at lower temperatures, as shown in **Figure 5a** [95–97].

It is generally accepted that on a standard TM catalyst, N_2 is largely adsorbed dissociatively on active sites that contain many metal atoms, like C7 or B5 sites on the surface of Fe or Ru, respectively. The active sites on Li_4RuH_6 and Ba_2RuH_6 are, however, constituted by the electron- and H-rich [RuH_6] anion and the Li or Ba cations surrounding it, and the long RuRu atomic distance defines why N_2 is not an adsorbate in a dissociative manner. A chemical alternative pathway was discovered through effective collaborative work with Vegge et al. Theoretical calculations on a Li_4RuH_6 model confirmed the (110) facet by showing an H-assisted associative activation of N_2 on the [RuH_6] center (**Figure 5b,c**). Firstly, N_2 adsorbs on the [RuH_6] site in an end-on complex. H^- is gradually carried to the polarized N-N antenna to generate a set of NxHy (x = 0–2, y = 0–3) intermediates by reducing it with protons of the surrounding Li cations. H_2 is then switched on to replenish the surface. It is the interaction of the transition metals, hydridic hydrogen, and alkali cations that allows the unique reaction pathway of the synthesis of ammonia with a short energy span of 1.75 eV, which prefers N_2 to NH_3 at

lower temperatures. This mechanism is experimentally supported by FTIR of adsorbed N_2 and NH_2 compounds, and tests involving $15N_2$-$14N_2$ isotope exchange [97–99].

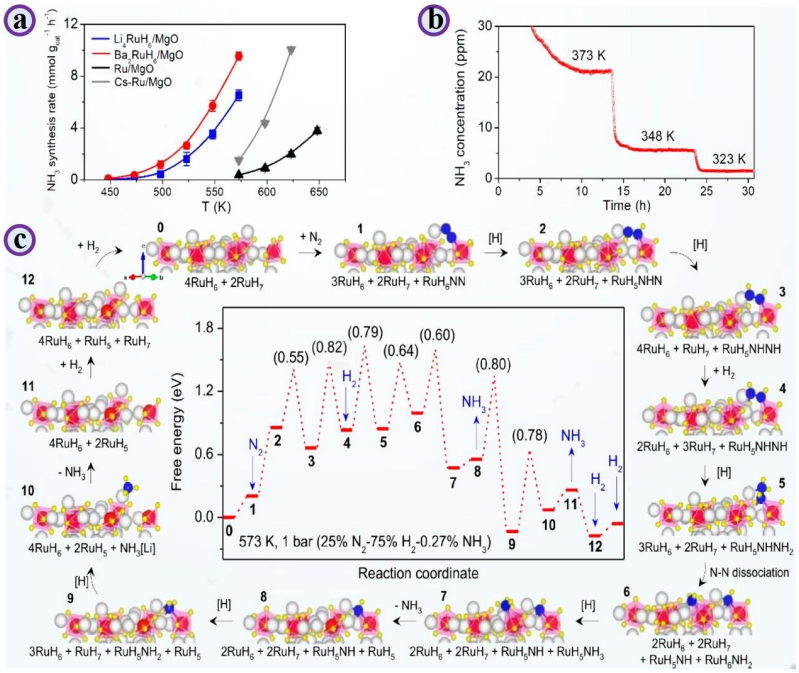

Figure 5. **(a)** Temperature-dependent NH_3 synthesis rate of various Ru catalysts at 0.1 MPa with H_2: N_2 = 3:1; **(b)** Time course effluent concentration of the ammonia synthesis of various Ru complex catalysts at 0.1 MPa with H_2N_2 = 1:3 and WHSV = 10800 $mLg^{-1}h^{-1}$; **(c)** calculates the free-energy pathway of the associative mechanism of ammonia synthesis over Ru complex catalysts [97].
Note: Color code: Ru: red, Li: white, H: yellow, N: blue.

3.4. Mixed-anion hydride catalysts

Recently, there has been a lot of interest in mixed-anion materials, including oxyhydrides and oxynitrides, because of their unusual characteristics, like rapid hydride ion conductivity, increased ferroelectric behavior, and significant catalytic activity [67, 100]. The kinetic and isotope exchange experiments showed that the hydrogen of the lattice in the $Ru/BaTiO_{2.5}H_{0.5}$ took part in the catalytic cycle, according to the Mars-van Krevelen mechanism of NH_3 formation (**Figure 6a**), and the phenomenon of hydrogen poisoning the catalyst was significantly reduced. His performance is higher than that of Co-based catalysts of the state of the art. The $BaAl_2O_{4-x}H_y$ has a stuffed tridymite structure and interstitial cage sites that contain anionic electrons. The surface of it has an ultralow work function (1.7–2.6 eV), and thus, it can strongly contribute to electron donation to Co, significantly reducing N_2 to NH_3 with the help of lattice H^- ions (**Figure 6b**). This three-dimensional, tetrahedrally built structure of the stuffed tridymite structure based on AlO_4 affords a high degree of chemical stability, which guards against oxidation of both the anionic electrons and hydrogen ions that are present in the structure. This structural strength guarantees a higher level of resistance to the environment and reusability of the catalysts compared to other reported hydride-based systems [101]. **Figure 6c** shows the Development of perovskite-type oxyhydrides such as Ru-loaded $BaCeO_{3-x}N_\gamma H_x$, enabling highly active ammonia synthesis, with N_2 dissociation on

$BaCeO_{3-x}N_\gamma H_x$ surfaces faster than N–H bond formation. Ru/$BaCeO_3$ follows a Langmuir–Hinshelwood mechanism where N_2 and H_2 are dissociatively adsorbed on Ru, with N_2 dissociation as the rate-determining step. For Ru/$BaCeO_{3-x}N_\gamma H_x$, Hosono et al. proposed a Mars–van Krevelen mechanism involving lattice N or anion-vacancy-activated N_2 reacting with lattice H^- to form NNH intermediates that hydrogenate to NH_3 [87].

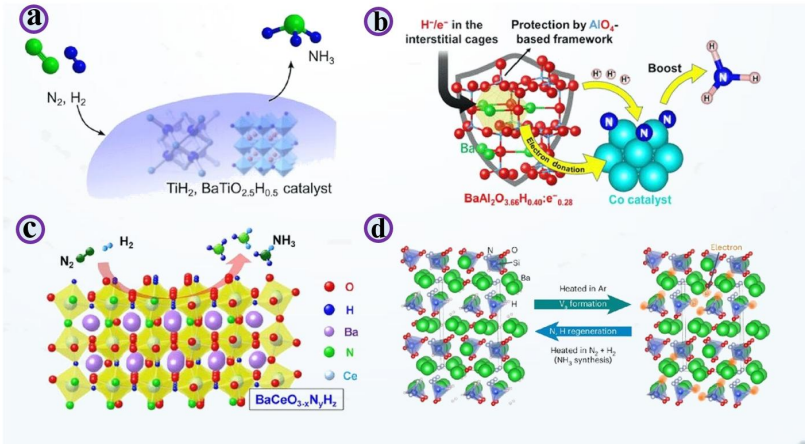

Figure 6. Schematics for catalytic ammonia synthesis over: **(a)** $BaTiO_{2.5}H_{0.5}$ [61]; **(b)** $BaAl_2O_{4-x}H_y$ [101]; **(c)** $BaCeO_{3-x}N_yH_z$ [67]; **(d)** $Ba_3SiO_{2.87}N_{0.80}H_{1.86}$ [102] and their supported catalysts.

The above oxyhydride or oxynitride-hydride catalysts all tend to have a transition metal site in their lattice structure or have the transition metal site on them as an active site, whereas in oxide materials containing no transition metal sites, there are very few effective catalysts. In the recent past, Kitano et al. have published a new orthosilicate oxynitride-hydride ($Ba_3SiO_{2.87}N_{0.80}H_{1.86}$) with ammonia synthesis capability through a catalytic reaction involving anion vacancy. The lattice can easily be desorbed to produce H^- and surface N_3^- anions under conditions of ammonia synthesis. The crystal has a great structural malleability, thus enabling it to produce and host a large number of electrons at anion vacancy sites. In the absence of any transition metal sites, these anion vacancies can directly activate N_2 molecules and generate ammonia in an associative hydrogenation reaction (**Figure 6d**).

3.5. Photo-driven ammonia synthesis using hydrides

The fact that solar energy is a renewable and plentiful resource has attracted a lot of interest among researchers in terms of artificial solar-driven chemical reactions and catalytic processes. Research has found that some alkali/alkaline earth metal hydrides are semiconducting [103,104]. It caused people to be immediately interested in studying the photon-hybrid interactions to trigger new chemical reactions [105]. Recently, Guan et al. found that LiH can be rapidly colored in the ultraviolet (UV) light as white turns to pale blue (**Figure 7a**) and that electron paramagnetic resonance (EPR) spectroscopy (**Figure 7b**) showed the occurrence of F-center defects (color centers) in the lattice of UV-irradiated LiH samples. The presence of this phenomenon suggests that LiH is dehydrogenated by UV radiation. Fourier-transform infrared spectroscopy

(FTIR) showed evidence of N-H stretching vibrations to be observed in samples of LiH when subjected to UV ray irradiation in the presence of N_2.

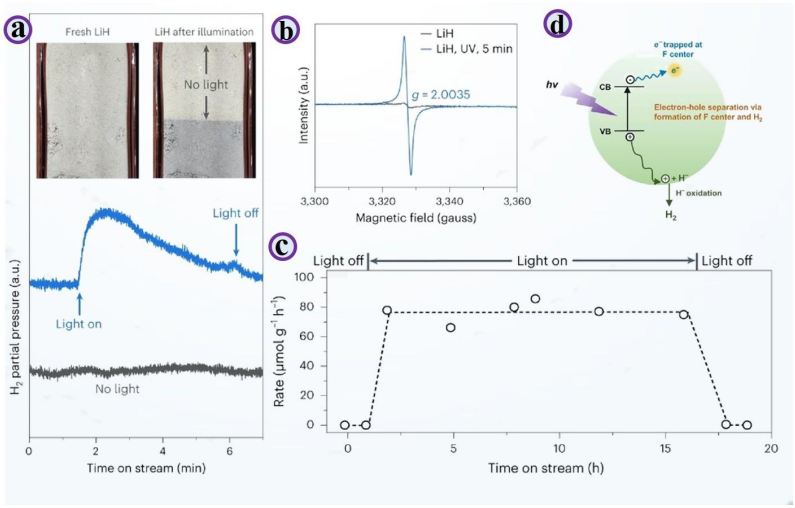

Figure 7. **(a)** Mass spectrometry of LiH with the presence or absence of UV light and the presence or absence of Ar at room temperature. Inset is the digital photographs of LiH under UV and no UV light, **(b)** LiH EPR spectra under illumination or no illumination. The rate is written as: **(c)** The rate of photocatalytic ammonia synthesis LiH during the UV irradiation; **(d)** Processing schemes of the charge carrier separation processes of the LiH photolysis process [106].

Follow-up measurements showed that introducing an N_2/H_2 feed with low H_2 content to LiH enables photocatalytic NH_3 formation under ambient-temperature illumination. Mechanistic analyses suggest that UV illumination generates electron–hole pairs; photogenerated holes oxidize H^- to form H_2, while electrons are trapped in long-lived color centers associated with hydrogen vacancies (**Figure 7d**). These trapped electrons facilitate N_2 activation and enable photo-switchable nitrogen conversion, allowing NH_3 formation without transition-metal catalysts. This work highlights hydrides as mediators for photocatalytic nitrogen fixation and suggests potential solar-driven routes for ammonia synthesis [106].

4. Chemical looping ammonia synthesis (CLAS)

4.1. Fundamental concepts and thermodynamics

Chemical looping ammonia synthesis (CLAS) separates NH_3 formation into sequential steps mediated by solid nitrogen carriers, reducing direct competition between N_2 and H_2 adsorption that constrains conventional single-surface catalysis. Depending on the hydrogen source, CLAS can operate as H_2O-CLAS (water as the hydrogen source) or H_2-CLAS (hydrogen gas). In H_2O-CLAS, metals first fix N_2 to form metal nitrides, which are then hydrolyzed to release NH_3 and form oxides that are subsequently reduced back to the metal. Thermodynamic analyses of hydride-based carriers indicate that nitrogen fixation to imide/nitride phases can be favorable over broad temperature windows (≈0–500 °C) for selected Li/Mg/Ca/Ba systems, while the corresponding hydrogenation steps are often endothermic and strongly dependent on carrier composition. These trends help identify hydride/imide pairs

that are both thermodynamically viable and potentially tunable for practical looping conditions [107–112].

4.2. Nitrogen carriers and advanced CLAS strategies

Experiments using LiH/Li_2NH and BaH_2/BaNH carrier pairs demonstrated CLAS at atmospheric pressure around 350 °C. Kinetic analysis indicated that nitrogen fixation has a substantially higher apparent activation barrier than the subsequent hydrogenation step, making carrier nitridation the rate-determining process in BaH_2/BaNH-mediated looping. Introducing transition metals (Fe, Co, Ni) markedly improved kinetics; Ni showed the strongest effect, reducing the apparent activation energy for nitrogen fixation (e.g., from ~109 to ~46 kJ mol^{-1} in Ni–BaH_2) and enabling measurable NH_3 formation at lower temperatures. Reported rates reached ~1533 and ~3125 μmol g^{-1} h^{-1} at 300 °C for Ni–LiH and Ni–BaH_2, respectively, and supporting Ni–BaH_2 on high-surface-area Al_2O_3 enabled NH_3 formation below 100 °C. Cycling tests also indicated multi-cycle operation, although phase segregation can contribute to activity decay shows in (**Figure 8a,b**).

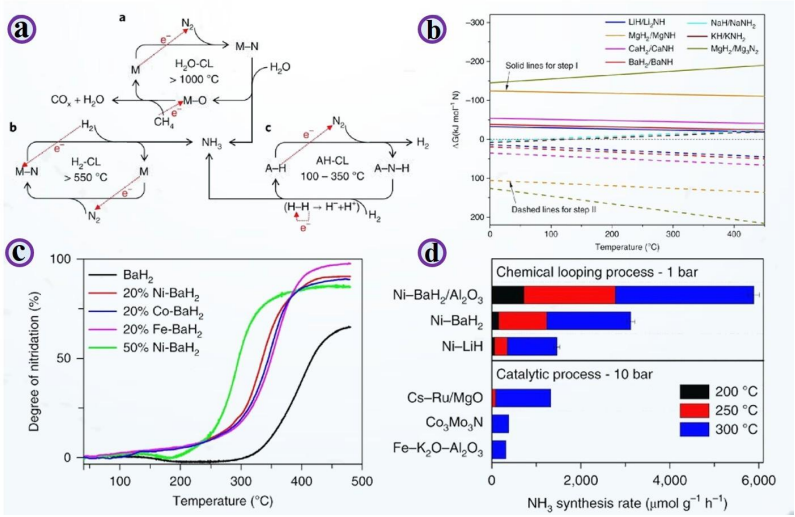

Figure 8. **(a)** A: H_2O-CL, B: H_2-CL, C: AH-CL (three different types of CLAS). Where M, A is metal and alkali/alkaline earth metal; **(b)** Thermodynamic investigations of processes I and II of AH-CL. TM catalyzed; **(c)** BaH_2 nitridation; **(d)** The rate of NH_3 in Ni-catalyzed AH-CL as compared to some of the active catalysts in the traditional thermocatalytic process [68].

More experiments demonstrated that ammonia production can be realized below 100 °C with the support of Ni-BaH_2 on the high-surface-area Al_2O_3. The Ni-BaH_2/Al_2O_3 CLAS performance in the ammonia synthesis reaction at 250 °C and 1 bar pressure was found to be an order of magnitude higher than the high-activity Cs-Ru/MgO catalyst under the same temperature and 10 bar pressure. And cycling tests were also performed on the Ni-BaH_2 sample, which showed that at least 10 cycles can be performed at 250 °C. The 10th cycle activity was nearly 80% of the original value. Additional studies found that the process of activity decay could be caused by phase segregation of Ni and BaH_2 following repeated cycles. Amazingly, re-ball milling the sample allowed restoring the activity to some extent shows in **Figure 8c,d** [68].

The CLAS process separates the ammonia synthesis into two or more consecutive stages through the use of nitrogen carriers [107]. This method is successful in overcoming the scaling relations of the single transition metal catalysts. CLAS does not require the competitive adsorption of N_2 and H_2 by step-wise feeding, as conventional catalytic methods of ammonia synthesis do. Also, the thermodynamics and the kinetics of each step may be optimized by adjusting the properties of the carriers of nitrogen [108]. A multifunctional composite nitrogen carrier was developed by Feng et al., which combined BaH_2/BaNH nitrogen carriers with the conventional nitride carriers (Mn_4N) (**Figure 9a**) [69]. Findings showed that Mn_4N not only catalyzes nitrogen fixation and ammonia release in the course of transformations of hydrogen and imides but also plays a secondary transport role in nitrogen through Mn_4N-Mn_2N conversion. This compound carrier pledged CLAS at 200–400 °C, where Mn_4N-BaH_2 gave a rate of ammonia synthesis of 3142 μmol g^{-1} h^{-1} at 300 °C, which was many times better than the performance of the individual carriers. Those outcomes of cycle stability indicate that the Mn_4N-BaH_2 performance is fundamentally stable after 6 complete cycles at 275 °C and atmospheric pressure. Moon et al. provide an in-situ neutron spectroscopy and diffraction analysis that is supported by first-principles simulations to examine the structural change throughout the nitridation and hydrogenation of Ni-BaH_2 [113]. They determined that ball-milling of the Ni-BaH_2 precursor triggers a dramatic reduction in the size of the BaH_2 particles and an increment of its defect density and potential elevation of its reactivity.

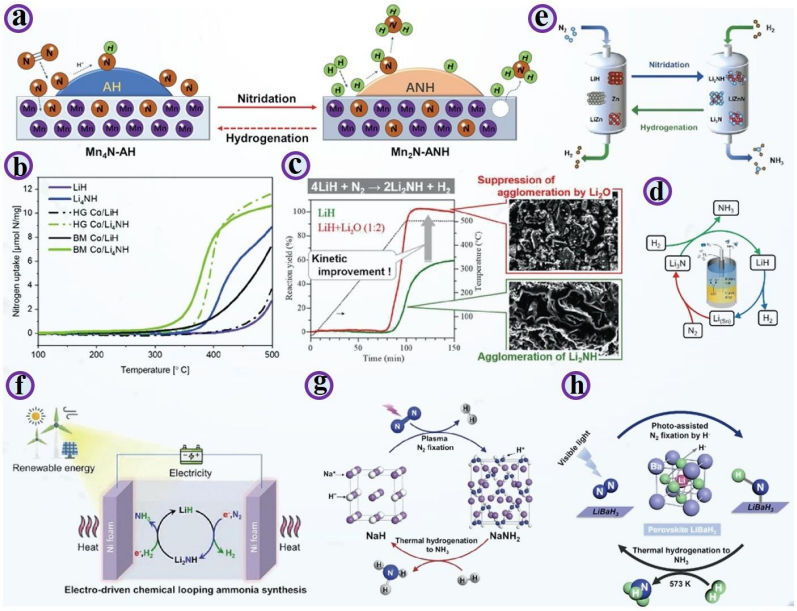

Figure 9. **(a)** The mediating scheme of CLAS with MnN_x-BaNH composite N carrier [69]; **(b)** N_2 -TPR of plain and cobalt-composite LiH and Li_4NH [114]; **(c)** The results of the LiH in the presence of Li_2O in the TG-MS reaction were compared with the results without Li_2O [114]; **(d)** CLAS: Molten LiCl-KCl eutectic molten Salt, Li-Sn alloy [115]; **(e)** Schematic diagram of the CLAS reaction mediated by ZnLiH-Li_2NH [116]; **(f)** Electro-directed CLAS reaction mediated by LiH/Li_2NH cycle Conceptual cycle [117]; **(g)** NaH/$NaNH_2$-mediated NaH/$NaNH_2$-mediated conceptual cycle of Plasma-driven CLAS [118]; **(h)** Photo-driven CLAS process mediated by $LiBaH_3$ Conceptual cycle [119].

The findings of inelastic neutron scattering and diffraction confirm the transformation of BaH_2 into BaNH when it reacts with N_2. In the hydrogenation, along with the recovery of the product of hydrogenation, a barium imide intermediate lacking nitrogen can be detected. It was found that hydrogenation is more difficult than the nitridation process compared to other catalysts, and this supports the preferential N_2 activation property of the Ni/BaH_2 catalyst. In the case of LiH, Yan et al. examined the impact of Pd on the CLAS mediated by LiH [120]. The LiH-Li_2NH reaction was modified by the formation of the tertiary Pd Li-Pd-H and Li-Pd alloys in the reaction, and the rate of the reaction was greatly accelerated. Makepeace et al. discovered that the compositions of Li-N-H over a wide range may be made through either solid-state synthesis or N_2 reaction [121]. LiH can be nitridated at 300–500 °C to form partially reduced imides of the general formula $Li_2 + {}_xNH$ ($0 \leq x \leq 2$), a solid solution of Li_2NH and Li_4NH [114]. The nitride-hydride (Li_4NH) reacts subsequently with N_2 by almost an order of magnitude faster than LiH under similar conditions to form imide and nitride phases (**Figure 9b**). Nevertheless, the mechanisms that regulate the transformation of LiH to $Li_2+{}_xNH$, and the theoretical ammonia yield when subjected to the hydrogenation process, are only poorly known. Ichikawa et al. found that Li_2O was ball-milled into LiH-Li_2NH, inhibiting reactant agglomeration to increase the kinetics of LiH in the fixation of nitrogen (**Figure 9c**) [122]. Tang et al. have created a lithium-based alloy cycle system of CLAS (**Figure 9d**) in which nitrogen reacts with a Li-Sn alloy at 510 °C to form Li_3N [115]. Li_3N is then dissolved in a LiCl-KCl eutectic salt, and then reacts with H_2 at 450 °C to produce LiH and generate NH_3. They were also able to determine that the formation of some intermediate species, like $LiNH_2$ or Li_2NH, was possible during the course of the reaction. According to Wang et al., Zn-LiH produced H_2 in the process of nitrogen fixing, which gave rise to many $LiZn_x$ intermetallic compounds and nitrogen-bearing species, including Li_2NH, Li_3N, and LiZnN (**Figure 9e**) [116]. In further hydrogenation, these species produced ammonia and returned to LiH, Zn, LiZn, and the CLAS cycle was concluded. Kinetic experiments demonstrated that Zn lowered the apparent activation energy of fixation of LiH nitrogen between 102 kJ mol^{-1} and 50 kJ mol^{-1}. Within 350 °C and atmospheric pressure, Zn-LiH generated ammonia 19 times faster than LiH, with a rate of 956 μmol g^{-1} h^{-1}.

The nitrogen fixation through hydrides is a process that is very different from the classic process of nitrogen activation on the transition metals. The study by Guan et al. aimed to examine the process of N_2 activation and transformation on BaH_2 by combining the theoretical and experimental methodologies [123]. Over the recent years, the use of electricity, light, plasma, etc., as external fields to drive CLAS processes has been studied by researchers, and significant progress has been made. Although CLAS catalyzed by the AH/ANH complexes may work at fairly mild conditions, at high temperatures, hydrogenation of ANH to ammonia is thermodynamically constrained. As an example, the concentration of ammonia in the equilibrium of the ANH hydrogenation process at 400 °C is just 626 ppm. In order to solve this problem, Feng et al. came up with an electro-driven LiH/Li_2NH-mediated H_2-CLAS process (**Figure 9f**) [117]. Hemodynamic studies showed that at room

temperature and pressure, as little as 0.05 V was required to raise the equilibrium concentration of ammonia in the course of Li_2NH hydrogenation between 0.19% and 8.5%. A voltage of 0.11 V at 400 °C and atmospheric pressure would increase the equilibrium concentration of ammonia to 27.1% further. This paper used molten salt electrolyte (LiCl-NaCl-KCl) to facilitate the two-step electrochemical reaction by electrical energy: nitridation of LiH and hydrogenation of Li_2NH. The experimental findings revealed that electrical energy contributed greatly to the hydrogenation of lithium imide as well as the fixation of nitrogen by lithium hydride; the apparent rate of the ammonia synthesis was increased by almost eight times relative to the thermochemical process. Moreover, such a technique theoretically provides better reaction thermodynamics than the existing Li^+-mediated electrochemical ammonia synthesis reactions and has been experimentally demonstrated to operate at low-voltage conditions (available currents up to 2.0 V). Wu et al. created a process of H_2-CLAS by a plasma-driven reaction between NaH (**Figure 9g**) [118]. As stated above, Guan et al. have found that lithium hydride (LiH) would mediate the process of photocatalytic ammonia production [69, 106]. These results indicate that external fields may have a major effect in enhancing the thermodynamic and kinetic performance of the CLAS process, resulting in ammonia production that is more efficient. Moreover, the combination of the external field-based processes with the storage and use of renewable energy may help develop the miniaturized and distributed ammonia production systems. Nevertheless, studies conducted by external fields to enhance CLAS are infrequent, and the mechanisms behind the beneficial effect are still unclear, posing tremendous opportunities in future research and advancements.

5. Thermocatalytic decomposition of ammonia

Over the past decade, substantial progress has been made in ammonia decomposition technologies aimed at producing high-purity, COx-free H_2 [19, 124–128]. Thermodynamically, NH_3 decomposition approaches near-complete equilibrium conversion at elevated temperatures (e.g., ~99% at 400 °C and ~99.7% at 500 °C), but residual NH_3 in the product stream can necessitate additional purification steps. Achieving scalable and energy-efficient cracking, therefore, depends on advances in three areas: highly active (preferably Ru-free) catalysts, efficient reactor designs, and integrated separation/purification strategies. Mechanistically, NH_3 decomposition proceeds through NH_3 adsorption, stepwise dehydrogenation to surface NHx species, and recombination/desorption of N_2 and H_2; catalyst choice strongly influences the rate-limiting steps and the operating temperature window [129–132].

This part discusses the kinetic and thermodynamic concepts of NH_3 breakdown on the basis of the appropriate examples explaining how various catalysts influence the process. Moreover, the NH_3 decomposition mechanisms, including the photodecomposition, electrochemical decomposition, and thermochemical decomposition, are also discussed in the article. The initial two have been briefly discussed, but the third one has been presented in detail, and a discussion about the kinetics, the processes involved in a reaction, the stability, and the catalytic efficiency has been presented. Further subsections address the purification of H_2 and the

separation processes involved in getting the N_2 out of the mixture of unreacted NH_3 and the generated H_2 [85] is shown in **Figure 10**.

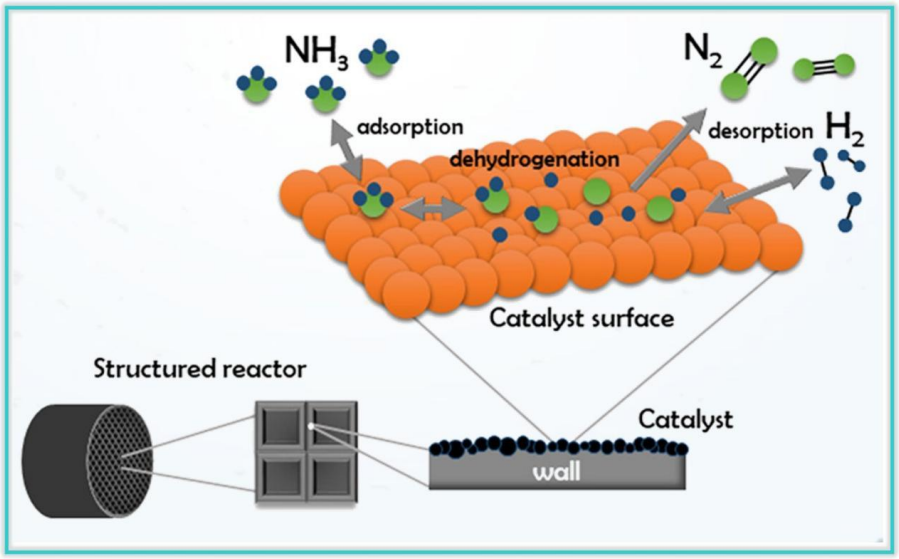

Figure 10. Decomposition of NH_3 into N_2 and H_2 via catalysis [133].

5.1. Amide- and imide-based catalysts

The breakdown of ammonia is also effective to produce green hydrogen, not contributing carbon because only nitrogen and hydrogen are emitted, which has attracted extensive interest. This reaction is thermodynamically preferred by the high temperatures (low pressures). Indicatively, when the temperature is at 400 °C, the conversion of ammonia can be at over 99% equilibrium (**Figure 11a**) [134]. The supported Ni-based catalysts in use today in industries demand temperatures over 700 °C to convert 99%. Thus, the creation of new and effective catalysts to decompose ammonia at moderate or low temperatures and the investigation of new processes will make the reaction temperatures and the use of energy even lower, allowing the mass production of ammonia decomposition technologies. The Sabatier principle indicates that the optimal catalyst to use in the decomposition of ammonia must possess an intermediate nitrogen adsorption energy. As in the case of ammonia synthesis catalysts, the activity of ammonia decomposition catalysts follows a volcano plot with respect to nitrogen dissociative adsorption energy (**Figure 11b**). Since Ru has a moderate energy of adsorption of nitrogen, it is positioned at the top of the curve and has the highest intrinsic activity. But the cost is high, and its availability is low, which limits its application; thus, the aim of finding alternative non-noble metal catalysts to Ru-based catalysts is a key area of concern in this sphere. Ammonia decomposition catalysts have been studied by researchers in great depth and volume within the past decades. The transition metals, alloys, metal nitrides, carbides, and sulfides are the major types of catalytic systems developed. The most promising have been group IX transition metals like Ru and Ni, and Mo or W nitride and carbide ammonia decomposers. Those who may want to learn more can use recent reviews on the same [135,136].

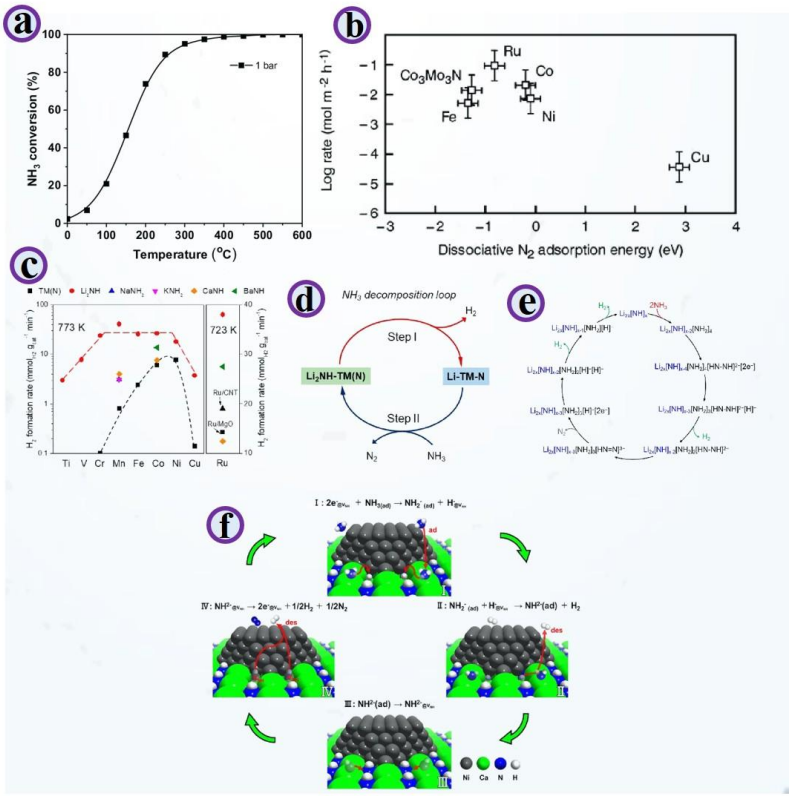

Figure 11. **(a)** At different temperatures, NH_3 was converted to equilibrium at 1 atm; **(b)** Experimental rate of ammonia decomposition with various catalysts as a function of reaction energy of dissociative N_2 adsorption [136]; **(c)** The decomposition rate of ammonia by selected transition metals in the presence of alkali/alkaline earth metals, amides/imides [90]; **(d)** Schematic representation of the mechanism of ammonia decomposition on TM-Li_2NH composite catalysts [90]; **(e)** The streamlined diagram of the catalytic ammonia decomposition process of Li_2NH [137]; **(f)** Schematic diagram explanation of the decomposition of ammonia on Ni/CaNH [81].

The possible use of alkali and alkaline earth metal imide compounds as hydrogen storage materials has influenced researchers to carry out thorough investigations of their structures, physicochemical characteristics, and chemical reactions [138]. Earlier on, in 1894, Tethered et al. found the degradation of ammonia to N_2 and H_2 when subjected to heated $NaNH_2$ that had attained a dark red color [139]. Chen et al. found in 2003 that $LiNH_2$ breaks down in the presence of temperatures higher than 400 °C, and releases gas-phase products that contained NH_3, N_2, and H_2 [140]. Scientists have thought that N_2 and H_2 could be a result of NH_3 decomposition, which is catalyzed by $LiNH_2$/Li_2NH. Using this finding, Guo et al. performed systematic and in-depth research on the alkali metal amides' participation in the ammonia decomposition. They discovered by extensive experimental validation that N_2 and H_2 do not directly result in catalytic decomposition of NH_3 by $LiNH_2$/Li_2NH but are closely associated with the stainless-steel reactor on which the test was conducted [141]. $LiNH_2$ decomposes at temperatures under 450 °C to produce mostly NH_3, the gaseous product in a quartz reactor. Within a stainless-steel reactor, however, it is possible to observe N_2 and H_2 signals below 300 °C of temperature, and $NaNH_2$ behaves in the same manner. This observation shows clearly that pure alkali metal amide or imide compounds have very

low levels of catalytic activity to decompose NH_3, and the presence of transition metals is important in catalyst imide/amide catalysis. At this time, David et al. had reported that $NaNH_2$ had a good exponential ammonia decomposition activity on stainless steel reactors [142].

The authors proposed the possibility of $NaNH_2$ as a new catalyst in ammonia decomposition, similar to the Ru-based catalysts. In 2015, Guo et al. synthesized a group of composite catalysts that incorporate Li_2NH and either transition metals or their nitrides (TM-Li_2NH) as the components [80]. **Figure 11c** demonstrates that the intrinsic activities of Ti, V, Cr, Mn, and Cu were low and had a volcano plot. Introduction of Li_2NH gave a big boost to the ammonia decomposition property of 3d transition metals, with Cr and Mn having their activity improved by 1 to 2 orders of magnitude, and Co and Ni, which are regarded as good catalysts in ammonia decomposition, improving activity by 2 to 3-fold. MnN-Li_2NH was the most active with a rate of Hydrogen permeation of 37.5 mmolH_2 $g_{cat}^{-1}min^{-1}$ at 500 °C, 40 times more active than MnN and similar to highly active Ru/CNTs [90,143]. In their paper on the alkali metal promoters in ammonia synthesis catalysts, Medford et al. theoretically showed that the introduction of promoters does not change the shape of the volcano curve [144]. In the TM(N)-Li2NH system, however, the activities of Li_2NH-promoted Cr, Mn, Fe, Co, and Ni catalysts were fairly close, and not like the volcano-shaped curve of pure 3d TM catalysts.

This observation indicates that the mechanism of decomposition of ammonia in this system is different from conventional ammonia decomposition by alkali metal-promotion of transition metals and their nitrides. According to the XRD, XAS, TPR, and the isotope experiment results, the authors have suggested a new two-step ammonia decomposition mechanism (**Figure 11d**). Firstly, Li_2NH is reacted with TM(N) to give ternary nitrides (LiTMN) and H_2. LiTMN, on the other hand, interacts with NH_3 to form Li_2NH and emits N_2 to form a complete catalytic cycle. In contrast to the conventional electronically promoted electronics, Li_2NH is an NH_3 transfer medium that allows the reaction to form transition metal nitride intermediates. In 2023, Yang et al. and Mambretti et al. made an ab initio molecular dynamics simulation (AIMD) discovery that shows that the dynamic surface structure variations of Li_2NH contribute to the catalytic ammonia decomposition behavior (**Figure 11e**) considerably [137,145]. In this situation, the surface composition and structure of Li_2NH are subjected to a sequence of dynamic processes that eventually cause the extraction of N_2 and H_2. Another point that is made in this research is the role of Li_2NH in ammonia breakdown as opposed to the orthodox role of alkali metals as electronic promoters. Besides the TM(N)-Li_2NH system, Guo et al. transferred these catalyst systems to other metals with alkali/alkaline earth metal amides/imides and prepared catalytic systems including Ru-$Ba(NH_2)_2$ [15], Mn_6N_5-CaNH [146], MnN-Li_2NH [147], Ni-$NaNH_2$ [148], and Ru-Li_2NH [149] with all of them showing excellent ammonia decomposition activity. Moreover, according to Kishida et al., the oblate-spherical Ru particles that are large and oblate in shape are efficient catalysts of the decomposition of ammonia in the presence of $Ca(NH_2)_2$ [150]. The characteristically increasing size of the particle of Ru resulted in a two-order increase in the TOF of Ru-Ca $(NH_2)_2$. The authors attributed

that being very active Ru-Ca $(NH_2)_2$, the shape and the optimal size of the particles of Ru, and the density of the active sites. Subsequently, they reported an effective ammonia decomposition reactor called Ni-CaNH catalyst that uses an NH_2^- vacancy based Mars-von Krevelen mechanism [81]. The ammonia decomposition activity of Ni-CaNH was found to have an operating temperature that is lower by 100 °C than in the reference Ni-based catalysts. The main locations of decomposition of ammonia, according to the results of the experimental and DFT calculations, are the VNH sites at the Ni-CaNH interface. To begin with, the VNH sites are created in the process of pretreatment. The addition of a 1:3 N_2/H_2 mixed gas stream leads to the oxidation of NH_2-species in the CaNH lattice to form N_2 and H_2 by the nickel catalyst, yielding VNH sites that have two anionic electrons in them. Next, the NH_3 breaks down at the VNH sites through a four-step reaction. In step I, the adsorption of NH_3 to the positively charged Ca^{2+} sites that surround the VNH sites and the reaction of the two anionic electron donors on the VNH sites to generate NH_2 anion and H anion take place. The reaction of the H-captured at the VNH site with a proton at the NH_2-site results in the production of H_2 and the generation of NH_2^-. In Step III, the formed NH_2^- fills in the VNH site. The NH_2^- lattice (IV) dissociates into N_2 and H_2 (step IV) and initiates the regeneration of the VNH sites at the Ni-CaNH interface (**Figure 11f**) [81]. These data indicate that NH_2^- vacancies on CaNH are highly significant in enhancing the reaction of decomposing ammonia. The above-discussed works and the findings provided evidence of a tremendous potential of alkali/alkaline earth metal amides and alkaline earth metal imides as catalysts in ammonia decomposition.

The thermodynamic properties of a catalytic reaction are crucial for the strategic development of catalysts with industrial relevance. The equation expresses the decomposition of NH_3 into H_2 and N_2:

$$2NH_3(g) \rightarrow N_2(g) + 3H_2(g),\ \Delta H = +46\ \text{kJ/mol}$$

Several theoretical works have reported on the relationship between temperature (250–700 °C) and the rate of NH_3 conversion (90–100%). Gibbs free energy is less, resulting in thermodynamic conversion of NH_3. The relationship between temperature and decomposition of NH_3 is not linear in the range of temperatures between 250–450 °C, yet the reaction rate does not considerably increase beyond 450 °C. Thus, in the high temperature regime, kinetic factors dominate the NH_3 breakdown. The awareness of these kinetic properties is pivotal in the establishment of effective catalytic devices, and how the process of breaking down takes place [151].

5.2. Hydride-mediated hydrogen production

Certain elements may form metal hydrides, particularly those in groups I–IV. These substances react readily with ammonia to produce a variety of amides/imides and nitrides. To create extensive amides, Bergstrom and Fernelius methodically compiled the reaction between an alkali metal and ammonia in 1933 [152]. The breakdown processes of these materials have been studied (**Table 2**), and SEM micrographs of the raw LiH **Figure 12a–d**. Kojima et al. have also examined the amides' capacity to be recycled. $LiNH_2$, $NaNH_2$, and KNH_2 spent 4, 4, and 2 h, respectively, in a hydrogen

flow environment (0.5 MPa). Then, samples were converted to LiH, NaH, and KH, respectively, in 96%, 100%, and 92% of cases [46,47,153]. Pure hydrogen can be made using the reaction between MH and NH_3 and later fed into a fuel cell once purified. Two hydrogen atoms in $LiNH_2$ are bound covalently to a nitrogen atom to produce the amide ion $[NH_2]^-$, which is in turn ionically bound to the Li-ion. As a result, the enthalpy of formation of $LiNH_2$ is less than that of ionic bonded hydrides, such as LiH; $LiNH_2$ breaks down at a relatively high temperature to yield the end product, Li_3N. The same trend can be noted with $NaNH_2$. Interestingly, both thermodynamic and kinetic considerations show that decomposition of the $Mg(NH_2)_2$ and $Ca(NH_2)_2$ is less stable when compared to that of $LiNH_2$. Thus, the electronegativity of the metal cation and the anion of the amide may affect the decomposition properties of the respective amide. Typically, Mg is more electronegative than Li or Na, and thus the ionic bond formed between Mg^{2+} and $[NH_2]^-$ is weaker than between Li^+ and $[NH_2]^-$, which explains the faster formation at the cost of the higher temperature decomposition observed with $LiNH_2$ than with other amides studied in this work. In addition, it was established that these metal hydrides are the ones that react with ammonia more easily, with a lower electronegativity of the metal cation. On the other hand, ammonia can be released more effectively by the formation of metal amides with cations possessing a greater value of the electronegativity [142].

Table 2. Metal Amide Synthesis by Ball Milling Reaction between Metal Hydrides and Gaseous NH_3.

Reaction	Time (h)	NH_3 pressure (MPa)	Decomposition temp (°C)
$LiH + NH_3 \rightleftharpoons LiNH_2 + H_2$	2	0.4	230–500
$NaH + NH_3 \rightleftharpoons NaNH_2 + H_2$	1	-	240–500
$KH + NH_3 \rightleftharpoons KNH_2 + H_2$	1	-	500–600
$MgH_2 + 2NH_3 \rightleftharpoons Mg(NH_2)_2 + 2H_2$	13	-	180–500
$CaH_2 + 2NH_3 \rightleftharpoons Ca(NH_2)_2 + 2H_2$	8	-	70–500

The design of a LiH-NH_3 hydrogen storage system with improved kinetic characteristics included a comprehensive investigation of the hydrogen desorption properties for reactions between lithium hydride with various particle sizes and NH_3 (0.5 MPa, NH_3/MH 1mol/mol) at 50–200 °C. Additionally, various potassium compounds were investigated as possible catalysts to enhance the system's hydrogen desorption reaction's kinetic characteristics. It is discovered that as the reaction temperature rises or the particle size of LiH decreases, the kinetic characteristics of the hydrogen desorption in the LiH-NH_3 system improve. **Figure 11** presents the hydrogen generation patterns of an hour at varying temperatures of raw LiH, ball-milled LiH, and KBr-enhanced LiH with NH_3 (0.5 MPa, NH_3/LiH = 1 mol/mol). The time-dependent hydrogen generation profiles for reactions carried out at 100 °C are offered in an inset of the figure. To improve the kinetic characteristics, KBr, KCl, KF, and KOH are useful; KBr has the most impact [49]. The hydrolysis-type reaction is exothermic; interestingly, the hydrogen desorption process may occur at ambient temperature. It has been shown that the response that recycles the by-product $LiNH_2$ back into LiH and NH_3 occurs at 300 °C when the partial pressure of NH_3 is lowered

under a 0.5 MPa flow of H_2 [46]. Ammonia must be converted to hydrogen at an average temperature in order for it to function as a hydrogen carrier. As a result, using what is already known, systems incorporating NH_3 and metal hydrides (MeH, where Me = Li, Na, K, Mg, and Ca) have been designed for this purpose. The reaction is formulated as follows [154, 155]. Moreover, several potassium-based substances were considered as possible catalysts, the goal of which was to increase the kinetic characteristics of the hydrogen desorption reaction of the system. The results were that the higher the temperature of the reaction or the size of the particles of LiH, the better the kinetic characteristics of desorption of hydrogen in the system LiH-NH_3. The compounds identified as most effective in enhancing these kinetic properties are KBr, KCl, KF, and KOH.

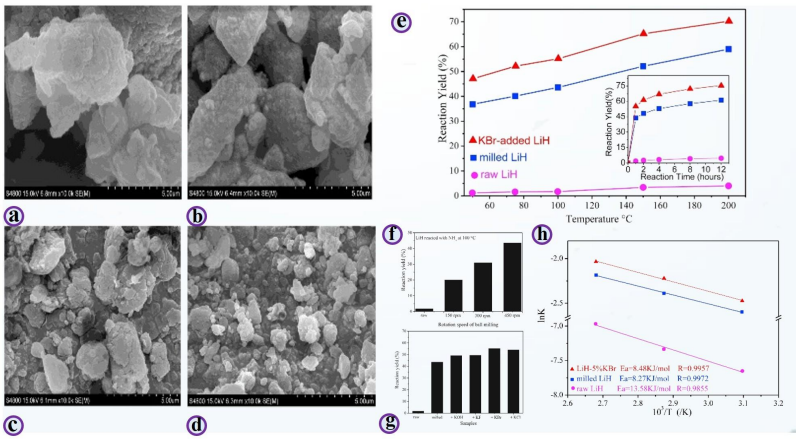

Figure 12. Hydrogen generation profile of the reaction of the raw LiH, ball-milled LiH, and the reaction of KBr-added LiH with NH_3: **(a–d)** SEM micrographs of the unprocessed LiH; **(e)** Percentage of reaction yield and the LiH ball-milled under rotation rates of 150 rpm, 300 rpm, and 450 rpm of 2 h; **(f–g)** Reaction yield on reactions between the raw LiH and the LiH ball-milled at various rotation speeds in the presence of NH_3 (0.5 MPa, NH_3/LiH = 1 mol/mol) at 100 °C with 1 h reaction time; **(h)** Arrhenius plot of the kinetic constant of the raw, ball-milled and KBr-added LiH at the measurement temperatures of 50, 75, 100, 150 and 200 °C [49].

$$MH + NH_3 \rightarrow MNH_2 + H_2 (M = Li, K, \text{and } Na) \quad (1)$$

5.3. Amide- and chemical looping–mediated hydrogen production

NH_3 suppression using various metal hydride additions. These systems, which have great volumetric and gravimetric hydrogen densities, are currently under investigation as materials to store hydrogen, such as LiNH, CaNH, Li/MgNH, and NaNH [138, 153, 156, 157]. This method is a significant difference from the previous surface catalytic practice since it involves the stoichiometric reduction and recovery of sodium amide ($NaNH_2$) through sodium metal. The Na/$NaNH_2$ system using 0.5 g of $NaNH_2$ and 60 sccm of NH_3 at 530 °C gives a 99.2% decomposition efficiency, which is favorable compared to other nickel and ruthenium-based catalysts in NH3 decomposition studies, which used a basic flow reactor. The development of $NaNH_2$-based ammonia cracking devices might increase the usage of NH_3 as a sustainable energy storage medium since it is an inexpensive and easily available substance. Sodium amide acts as a very effective catalyst for the stoichiometric

breakdown of ammonia, generating $NaNH_2$ from sodium metal. With an eye on sustainable energy applications, this technique departs from traditional transition metal catalysis by presenting a new class of amide-based materials for hydrogen extraction from ammonia. At different temperatures, the $NaNH_2$ decomposition efficiency of the supported ruthenium catalyst is shown in **Figure 13a**, which performs better at higher conversion levels [142]. Transition metals are the main catalysts for low-temperature NH_3 cracking; ruthenium has the best catalytic efficiency.

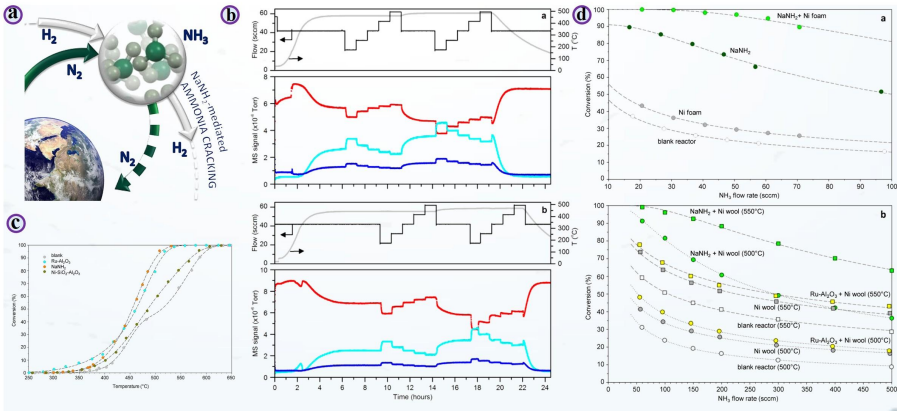

Figure 13. **(a)** Ammonia decomposition mechanism; **(b)** Results of the mass spectrometry of NH_3 (17, red), H_2 (2, cyan), and N_2 (28, blue) of the reaction of 0.25 g of $NaNH_2$ and 0.15 g of Na. The rates of temperature (light gray) and the flow rate of NH_3 (dark gray) in the course of the experiment at atmospheric pressure are shown in the upper pane of a given reaction; **(c)** Comparison of the NH_3 conversion; **(d)** Impact of containment methods and conversions obtained at different SCCM flow [142].

When the metal is incorporated with promoter species into complex support structures, its efficiency is significantly enhanced [158–161]. For the continuous stoichiometric breakdown of NH_3, sodium amide works equally well as a supported ruthenium catalyst, but at a far cheaper cost of materials. Given its reasonable cost and excellent efficiency, the $Na/NaNH_2$ system may constitute a novel class of NH_3 decomposition catalysts. Because of this potential, NH_3 decomposition should be given a second look as a practical hydrogen delivery technique for various purposes, including large-scale grid balancing, transportation, and distributed power production [162]. The mass spectrometry traces 0.25 g of NH_3 (red, m/z = 17), H_2 (cyan, m/z = 2), and N_2 (blue, m/z = 28) of the reaction of 0.25 g of $NaNH_2$ and 0.15 g of Na (**Figure 13b**). The temperature (light gray) and rate of flow of NH_3 (dark gray) in the course of the experiment at atmospheric pressure are shown in the upper panels of each reaction. Effects of containment techniques. conversion time (**Figure 13c**) time to obtain conversion of 0.5 g of $NaNH_2$ at 475 °C under a flow of 0.2 and 100 sccm in a reactor with a height of 1.6 mm and 1.141 cm^3. The reference data of blank reactor, Ni foam (only), and 0.5 g of $NaNH_2$ (only) are presented. Conversion at higher flows (50–500 sccm) of NH_3, in a 21.3 cm^3 reactor, of 0.5 g of $NaNH_2$ (green symbols), at 0.500 °C (solid circles) and 0.600 °C (solid squares) in the presence of 2 g nickel wool (**Figure 13d**). It is shown that the (i) alumina-supported ruthenium (2 g of nickel wool) (yellow symbols), (ii) 2 g of nickel wool (only) (gray symbols), and (iii) blank reactor data (open symbols) may be used as a reference.

The CLADH concept proceeds in two coupled steps. First, metallic Na (or K) reacts with NH_3 to form $NaNH_2$ (or KNH_2) while releasing one-third of the hydrogen. Second, the amide decomposes to regenerate the alkali metal with concomitant N_2 and H_2 formation, completing the loop. Thermodynamic analysis indicates that the ammoniation reactions are feasible below ~342 °C (Na) and ~301 °C (K), whereas amide decomposition to regenerate Na/K becomes favorable above ~275 °C ($NaNH_2$) and ~252 °C (KNH_2) under relevant gas atmospheres. Moreover, at sufficiently high temperatures, the Gibbs free energy for amide decomposition can be more favorable than direct NH_3 decomposition, suggesting a stronger driving force for hydrogen generation via the looping route. Experimental characterization (e.g., XRD/FTIR before and after reaction) supports room-temperature ammoniation to form amides and high-temperature amide decomposition to regenerate the metals. Adding MnN accelerates both stages, increasing hydrogen production rates by more than an order of magnitude relative to the pure amides under comparable conditions, as shown in **Figure 14a–d**.

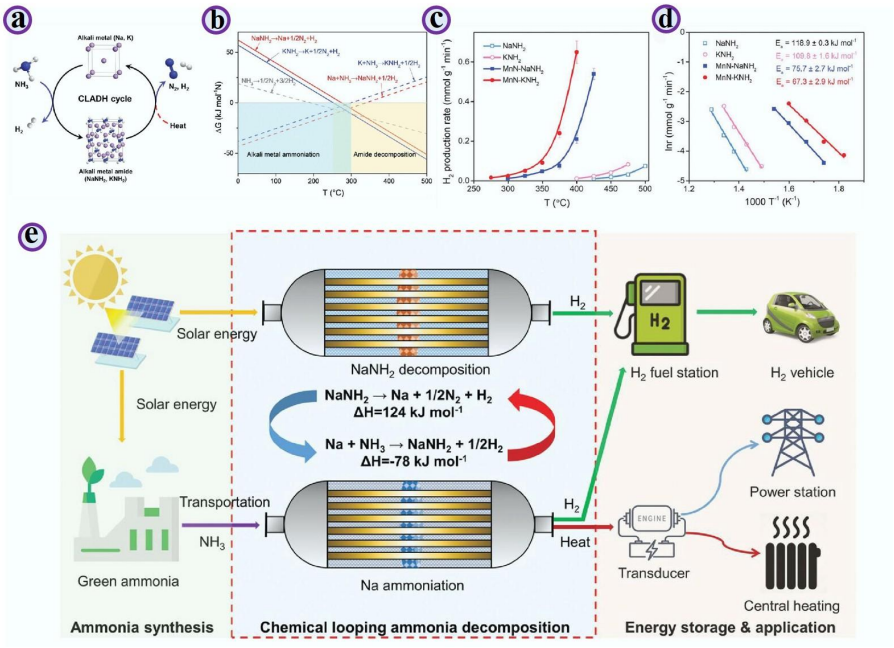

Figure 14. **(a)** Schematic scheme of CLADH with the use of alkali metals and all the corresponding pairs of alkali metals and amides; **(b)** Thermodynamics of CLADH. The solid curves are the temperature dependence of Gibbs free energy **(a–g)** of the degradation of $NaNH_2$ and KNH_2; **(c–d)** Temperature dependence of hydrogen production rates of CLADH [22]; The Arrhenius plot of the temperature-dependent rate of hydrogen production over $NaNH_2$ and KNH_2 with or without MnN; **(e)** CLADH process on the production of hydrogen and the storage of solar energy [163].

With MnN addition, hydrogen production was observed at temperatures as low as ~275–300 °C, consistent with a large decrease in apparent activation energy. At 400 °C, MnN–KNH_2 produced H_2 at ~0.65 mmol g^{-1} min^{-1} (≈59 × faster than KNH_2), and at 425 °C MnN–$NaNH_2$ reached ~0.54 mmol g^{-1} min^{-1} (≈54 × faster than $NaNH_2$). The apparent activation energies decreased to ~67.3 and ~75.7 kJ mol^{-1} for KNH_2 and $NaNH_2$, respectively, indicating a strong MnN–amide synergy. Under optimized

CLADH conditions, near-complete amide conversion was achieved (≈99% for KNH_2 at 400 °C and ≈98% for $NaNH_2$ at 425 °C). By contrast, when MnN–amide materials are evaluated under conventional thermal catalytic NH_3 decomposition conditions (i.e., without operating the full looping sequence), much lower net conversion is observed (reported as ~7% and ~13%), highlighting that the high performance is specific to the looping pathway, as shown in **Figure 14e** [22,163,164].

6. Conclusion

Alkali and alkaline-earth metal hydrides, amides, and imides have emerged as a versatile materials family for ammonia synthesis and decomposition, not merely as inert supports or promoters but as dynamic participants that store, transfer, and activate hydrogen and nitrogen. Across the studies reviewed here, a common theme is that these materials enable reaction pathways that differ from classical transition-metal surface chemistry: lattice hydride and interfacial hydride/electron transfer can facilitate heterolytic H_2 activation, stabilize reactive NxHy intermediates, and, in favourable cases, relax scaling constraints that limit metal-only catalysts. These features underpin advances in thermocatalytic ammonia synthesis using hydride/oxyhydride/complex hydride phases, photo-assisted routes in which hydrides generate long-lived charge carriers that promote nitrogen conversion, and chemical-looping schemes that separate nitrogen fixation and hydrogenation to reduce competitive adsorption and tune thermodynamic driving forces. For ammonia decomposition, amide/imide chemistry and looping-type concepts offer promising routes to COx-free hydrogen, with the additional advantage that operating modes can be designed to manage equilibrium limitations and mitigate residual NH_3 when paired with suitable purification strategies.

Despite clear progress, several barriers must be addressed to translate hydride/amide/imide-enabled chemistry into practical, scalable technologies. First, many of these materials are highly sensitive to air and moisture, and their long-term stability under realistic feeds (including trace contaminants) and repeated thermal cycling remains insufficiently understood. Second, performance often depends on evolving multiphase microstructures and interfaces (e.g., metal–hydride contacts, nitride/amide gradients, segregating promoters), yet these dynamic features are rarely controlled deliberately, leading to variability in activity and deactivation through sintering, phase separation, volatilization of carriers, or loss of active interfacial area. Third, while chemical-looping approaches demonstrate compelling thermodynamic and kinetic advantages, overall process efficiency will hinge on integrating fast solid-state transport, rapid gas–solid reaction steps, and energy-efficient heat management at scale. Finally, mechanistic interpretations are frequently inferred from ex situ characterization; robust operando evidence is still limited for key steps such as N_2 activation sites, hydride migration pathways, and the identity of dominant NxHy intermediates under working conditions.

Future research should therefore prioritize four directions. (1) Stabilize materials and interfaces: develop protective architectures (core–shells, passivation layers that remain permeable to $H_2/N_2/NH_3$), compositional tuning to suppress volatility, and supports/porous scaffolds that preserve interfacial contact and resist sintering. (2)

Mechanism-resolved design: combine isotopic labeling with operando spectroscopy and diffraction (e.g., in situ XRD/neutron methods, XAS, DRIFTS/IR, solid-state NMR where feasible) to quantify hydride and nitrogen mobility, identify rate-limiting steps, and distinguish true catalytic cycles from stoichiometric conversion. (3) Rational promotion and microstructure control: move beyond empirical promoter selection by mapping how alkali/alkaline-earth species, transition metals, and defects (vacancies, colour centres, oxyhydride composition) control electron/hydride transfer and adsorption energetics; design catalysts where the active phase and the active interface are engineered reproducibly. (4) Process and reactor integration: for thermocatalysis, couple catalysts to intensified reactors and downstream purification tailored to ultra-low residual NH_3; for photo-assisted routes, improve light harvesting and charge utilization while quantifying solar-to-chemical efficiencies; for chemical looping, optimize cycle scheduling, particle engineering, and heat integration, and evaluate system-level metrics (energy efficiency, durability, safety, and cost) against incumbent Haber–Bosch and conventional cracking.

Overall, hydride/amide/imide chemistry provides a powerful framework for rethinking ammonia as both a product and an energy vector. Continued progress will require aligning fundamental mechanistic insight with materials stabilization and process engineering so that the most promising laboratory demonstrations evolve into robust, efficient, and scalable platforms for low-carbon ammonia production and COx-free hydrogen delivery.

Author contributions: MAA, SH, and IUK conceived the idea, MAA and SH collected data, and wrote the first draft. IUK carried out data analysis and revised the manuscript. The whole project was administrated and supervised by the IUK. All authors have read and agreed to the published version of the manuscript.

Funding: This work received no external funding.

Institutional review board statement: Not applicable.

Informed consent statement: Not applicable.

Data availability statement: Not applicable.

Conflict of interest: The authors declare no conflict of interest.

References

1. Matthews HD, Wynes S. Current global efforts are insufficient to limit warming to 1.5 °C. Science. 2022; 376(6600): 1404–1409.
2. Aslam MA, Mustaqeem M, Abbas MS, et al. Hydrogen Revolution: Advances in Catalytic Ammonia Decomposition. Clean Energy Technologies. 2025; 1(1): 49–69.
3. Møller KT, Jensen TR, Akiba E, et al. Hydrogen-A sustainable energy carrier. Progress in Natural Science: Materials International. 2017; 27(1): 34–40.
4. He T, Pachfule P, Wu H, et al. Hydrogen carriers. Nature Reviews Materials. 2016; 1(12): 1–17.
5. Cha J, Park Y, Brigljević B, et al. An efficient process for sustainable and scalable hydrogen production from green ammonia. Renewable and Sustainable Energy Reviews. 2021; 152: 111562.
6. Aslam MA, Abbas MS, Irfan RM, et al. From ammonia to hydrogen: Evolution of ruthenium-based catalysts. ACS

Catalysis. 2025; 15(21): 18631–18662.
7. Liu M, Yao Z, Gu J, et al. Issues and opportunities facing hydrolytic hydrogen production materials. Chemical Engineering Journal. 2023; 461: 141918.
8. Dotan H, Landman A, Sheehan SW, et al. Decoupled hydrogen and oxygen evolution by a two-step electrochemical–chemical cycle for efficient overall water splitting. Nature Energy. 2019; 4(9): 786–795.
9. Hodges A, Hoang AL, Tsekouras G, et al. A high-performance capillary-fed electrolysis cell promises more cost-competitive renewable hydrogen. Nature Communications. 2022; 13(1): 1304.
10. Hauch A, Küngas R, Blennow P, et al. Recent advances in solid oxide cell technology for electrolysis. Science. 2020; 370(6513): eaba6118.
11. Clark D, Malerød-Fjeld H, Budd M, et al. Single-step hydrogen production from NH_3, CH_4, and biogas in stacked proton ceramic reactors. Science. 2022; 376(6591): 390–393.
12. Simagina VI, Vernikovskaya NV, Komova OV, et al. Experimental and modeling study of ammonia borane-based hydrogen storage systems. Chemical Engineering Journal. 2017; 329: 156–164.
13. Sørensen RZ, Hummelshøj JS, Klerke A, et al. Indirect, reversible high-density hydrogen storage in compact metal ammine salts. Journal of the American Chemical Society. 2008; 130(27): 8660–8668.
14. Humphries TD, Sheppard DA, Buckley CE. Recent advances in the 18-electron complex transition metal hydrides of Ni, Fe, Co and Ru. Coordination Chemistry Reviews. 2017; 342: 19–33.
15. Yu P, Guo J, Liu L, et al. Effects of alkaline earth metal amides on Ru in catalytic ammonia decomposition. The Journal of Physical Chemistry C. 2016; 120(5): 2822–2828.
16. Wang P, Chang F, Gao W, et al. Breaking scaling relations to achieve low-temperature ammonia synthesis through LiH-mediated nitrogen transfer and hydrogenation. Nature Chemistry. 2017; 9(1): 64–70.
17. Chang F, Tezsevin I, de Rijk JW, et al. Potassium hydride-intercalated graphite as an efficient heterogeneous catalyst for ammonia synthesis. Nature Catalysis. 2022; 5(3): 222–230.
18. Yin S, Xu B, Zhou X, et al. A mini-review on ammonia decomposition catalysts for on-site generation of hydrogen for fuel cell applications. Applied Catalysis A: General. 2004; 277(1–2): 1–9.
19. Schüth F, Palkovits R, Schlögl R, et al. Ammonia as a possible element in an energy infrastructure: catalysts for ammonia decomposition. Energy & Environmental Science. 2012; 5(4): 6278–6289.
20. Wan Z, Tao Y, Shao J, et al. Ammonia as an effective hydrogen carrier and a clean fuel for solid oxide fuel cells. Energy Conversion and Management. 2021; 228: 113729.
21. Le TA, Do QC, Kim Y, et al. A review on the recent developments of ruthenium and nickel catalysts for CO x-free H_2 generation by ammonia decomposition. Korean Journal of Chemical Engineering. 2021; 38(6): 1087–1103.
22. Feng S, Gao W, Guo J, et al. Progress of metal hydrides, amides and imides for ammonia synthesis and decomposition. The Innovation Energy. 2025; 100122-1–100122-18.
23. MacFarlane DR, Cherepanov PV, Choi J, et al. A roadmap to the ammonia economy. Joule. 2020; 4(6): 1186–1205.
24. Morlanés N, Katikaneni SP, Paglieri SN, et al. A technological roadmap to the ammonia energy economy: Current state and missing technologies. Chemical Engineering Journal. 2021; 408: 127310.
25. Mukherjee S, Devaguptapu SV, Sviripa A, et al. Low-temperature ammonia decomposition catalysts for hydrogen generation. Applied Catalysis B: Environmental. 2018; 226: 162–181.
26. Fang H, Wu S, Ayvali T, et al. Disperced surface Ru ensembles on MgO (111) for catalytic ammonia decomposition. Nature Communications. 2023; 14(1): 647.
27. Tabassum H, Mukherjee S, Chen J, et al. Hydrogen generation via ammonia decomposition on highly efficient and stable Ru-free catalysts: approaching complete conversion at 450 °C. Energy & Environmental Science. 2022; 15(10): 4190–4200.
28. Xie P, Yao Y, Huang Z, et al. Highly efficient decomposition of ammonia using high-entropy alloy catalysts. Nature Communications. 2019; 10(1): 4011.
29. Fang H, Liu D, Luo Y, et al. Challenges and opportunities of Ru-based catalysts toward the synthesis and utilization of ammonia. ACS Catalysis. 2022; 12(7): 3938–3954.
30. Cerrillo JL, Morlanés N, Kulkarni SR, et al. High purity, self-sustained, pressurized hydrogen production from ammonia in a catalytic membrane reactor. Chemical Engineering Journal. 2022; 431: 134310.
31. Maleki H, Fulton M, Bertola V. Kinetic assessment of H_2 production from NH_3 decomposition over CoCeAlO catalyst in a microreactor: Experiments and CFD modelling. Chemical Engineering Journal. 2021; 411: 128595.
32. Lee J, Ga S, Lim D, et al. Carbon-free green hydrogen production process with induction heating-based ammonia decomposition reactor. Chemical Engineering Journal. 2023; 457: 141203.

33. Brunauer S, Love KS, Keenan RG. Adsorption of nitrogen and the mechanism of ammonia decomposition over iron catalysts. Journal of the American Chemical Society. 1942; 64(4): 751–758.
34. Novell-Leruth G, Valcárcel A, Pérez-Ramírez J, et al. Ammonia dehydrogenation over platinum-group metal surfaces. Structure, stability, and reactivity of adsorbed NH_x species. The Journal of Physical Chemistry C. 2007; 111(2): 860–868.
35. Lorenzut B, Montini T, Pavel CC, et al. Embedded $Ru@ZrO_2$ catalysts for H_2 production by ammonia decomposition. ChemCatChem. 2010; 2(9): 1096–1106.
36. Niu L, Liu X, Zhou X, et al. Genesis of an $Fe_5C_2@Fe_3O_4$ core/shell structure during CO carburization of metallic iron nanoparticles. Journal of Catalysis. 2022; 407: 97–103.
37. Wang L, Zhao Y, Liu C, et al. Plasma driven ammonia decomposition on a Fe-catalyst: eliminating surface nitrogen poisoning. Chemical Communications. 2013; 49(36): 3787–3789.
38. Okura K, Okanishi T, Muroyama H, et al. Ammonia decomposition over nickel catalysts supported on rare-earth oxides for the on-site generation of hydrogen. ChemCatChem. 2016; 8(18): 2988–2995.
39. Im Y, Muroyama H, Matsui T, et al. Ammonia decomposition over nickel catalysts supported on alkaline earth metal aluminate for H_2 production. International Journal of Hydrogen Energy. 2020; 45(51): 26979–26988.
40. Duan X, Ji J, Yan X, et al. Understanding Co-Mo catalyzed ammonia decomposition: influence of calcination atmosphere and identification of active phase. ChemCatChem. 2016; 8(5): 938–945.
41. Podila S, Driss H, Zaman SF, et al. MgFe and Mg–Co–Fe mixed oxides derived from hydrotalcites: highly efficient catalysts for CO_x free hydrogen production from NH_3. International Journal of Hydrogen Energy. 2020; 45(1): 873–890.
42. Leybo DV, Baiguzhina AN, Muratov DS, et al. Effects of composition and production route on structure and catalytic activity for ammonia decomposition reaction of ternary Ni–Mo nitride catalysts. International Journal of Hydrogen Energy. 2016; 41(6): 3854–3860.
43. Zamfirescu C, Dincer I. Using ammonia as a sustainable fuel. Journal of Power Sources. 2008; 185(1): 459–465.
44. Klerke A, Christensen CH, Nørskov JK, et al. Ammonia for hydrogen storage: challenges and opportunities. Journal of Materials Chemistry. 2008; 18(20): 2304–2310.
45. Miyaoka H, Ichikawa T, Hino S, et al. Compressed hydrogen production via reaction between liquid ammonia and alkali metal hydride. International Journal of Hydrogen Energy. 2011; 36(14): 8217–8220.
46. Kojima Y, Tange K, Hino S, et al. Molecular hydrogen carrier with activated nanohydride and ammonia. Journal of Materials Research. 2009; 24: 2185–2190.
47. Yamamoto H, Miyaoka H, Hino S, et al. Recyclable hydrogen storage system composed of ammonia and alkali metal hydride. International Journal of Hydrogen Energy. 2009; 34(24): 9760–9764.
48. Hino S, Ogita N, Udagawa M. Thermodynamic properties of lithium amide under hydrogen pressure determined by Raman spectroscopy. Journal of Applied Physics. 2009; 105(2): 023521.
49. Dong BX, Song L, Teng YL, et al. Enhanced hydrogen desorption reaction kinetics by optimizing the reaction conditions and doping potassium compounds in the $LiH–NH_3$ system. International Journal of Hydrogen Energy. 2014; 39(25): 13838–13843.
50. Kitano M, Inoue Y, Yamazaki Y, et al. Ammonia synthesis using a stable electride as an electron donor and reversible hydrogen store. Nature Chemistry. 2012; 4(11): 934–940.
51. Kitano M, Inoue Y, Ishikawa H, et al. Essential role of hydride ion in ruthenium-based ammonia synthesis catalysts. Chemical Science. 2016; 7(7): 4036–4043.
52. Abe H, Niwa Y, Kitano M, et al. Anchoring bond between Ru and N atoms of Ru/Ca_2NH catalyst: crucial for the high ammonia synthesis activity. The Journal of Physical Chemistry C. 2017; 121(38): 20900–20904.
53. Gong Y, Wu J, Kitano M, et al. Ternary intermetallic LaCoSi as a catalyst for N_2 activation. Nature Catalysis. 2018; 1(3): 178–185.
54. Li J, Wu J, Wang H, et al. Acid-durable electride with layered ruthenium for ammonia synthesis: boosting the activity via selective etching. Chemical Science. 2019; 10(22): 5712–5718.
55. Ye TN, Park SW, Lu Y, et al. Vacancy-enabled N_2 activation for ammonia synthesis on an Ni-loaded catalyst. Nature. 2020; 583(7816): 391–395.
56. Ye TN, Lu Y, Kobayashi Y, et al. Efficient ammonia synthesis over phase-separated nickel-based intermetallic catalysts. The Journal of Physical Chemistry C. 2020; 124(52): 28589–28595.
57. Zhang K, Cao A, Wandall LH, et al. Spin-mediated promotion of Co catalysts for ammonia synthesis. Science. 2024; 383(6689): 1357–1363.

58. Yiliguma, Park SW, Li J, et al. C_2 vacancy-mediated N_2 activation over Ni-loaded rare-earth dicarbides for ammonia synthesis. ACS Catalysis. 2021; 11(12): 7595–7603.
59. Wang Q, Guan Y, Guo J, et al. Hydrides mediate nitrogen fixation. Cell Reports Physical Science. 2022; 3(3): 100796.
60. Chang F, Guan Y, Chang X, et al. Alkali and alkaline earth hydrides-driven N2 activation and transformation over Mn nitride catalyst. Journal of the American Chemical Society. 2018; 140(44): 14799–14806.
61. Kobayashi Y, Tang Y, Kageyama T, et al. Titanium-based hydrides as heterogeneous catalysts for ammonia synthesis. Journal of the American Chemical Society. 2017; 139(50): 18240–18246.
62. Wang Q, Pan J, Guo J, et al. Ternary ruthenium complex hydrides for ammonia synthesis via the associative mechanism. Nature Catalysis. 2021; 4(11): 959–967.
63. Yamashita H, Broux T, Kobayashi Y, et al. Chemical pressure-induced anion order–disorder transition in LnHO enabled by hydride size flexibility. Journal of the American Chemical Society. 2018; 140(36): 11170–11173.
64. Zhang X, Liu L, Wu A, et al. Synergizing surface hydride species and Ru clusters on Sm_2O_3 for efficient ammonia synthesis. ACS Catalysis. 2022; 12(4): 2178–2190.
65. Mao C, Wang J, Zou Y, et al. Hydrogen spillover to oxygen vacancy of TiO_2–xH_y/Fe: breaking the scaling relationship of ammonia synthesis. Journal of the American Chemical Society. 2020; 142(41): 17403–17412.
66. Guan Y, Zhang W, Wang Q, et al. Barium chromium nitride-hydride for ammonia synthesis. Chem Catalysis. 2021; 1(5): 1042–1054.
67. Kitano M, Kujirai J, Ogasawara K, et al. Low-temperature synthesis of perovskite oxynitride-hydrides as ammonia synthesis catalysts. Journal of the American Chemical Society. 2019; 141(51): 20344–20353.
68. Gao W, Guo J, Wang P, et al. Production of ammonia via a chemical looping process based on metal imides as nitrogen carriers. Nature Energy. 2018; 3(12): 1067–1075.
69. Feng S, Gao W, Wang Q, et al. A multi-functional composite nitrogen carrier for ammonia production via a chemical looping route. Journal of Materials Chemistry A. 2021; 9(2): 1039–1047.
70. Deng QF, Zhang H, Hou XX, et al. High-surface-area $Ce_{0.8}Zr_{0.2}O_2$ solid solutions supported Ni catalysts for ammonia decomposition to hydrogen. International Journal of Hydrogen Energy. 2012; 37(21): 15901–15907.
71. Huang C, Yu Y, Tang X, et al. Hydrogen generation by ammonia decomposition over Co/CeO2 catalyst: Influence of support morphologies. Applied Surface Science. 2020; 532: 147335.
72. Nagaoka K, Eboshi T, Abe N, et al. Influence of basic dopants on the activity of Ru/Pr_6O_{11} for hydrogen production by ammonia decomposition. International Journal of Hydrogen Energy. 2014; 39(35): 20731–20735.
73. Okura K, Okanishi T, Muroyama H, et al. Promotion effect of rare-earth elements on the catalytic decomposition of ammonia over Ni/Al_2O_3 catalyst. Applied Catalysis A: General. 2015; 505: 77–85.
74. Lu AH, Nitz JJ, Comotti M, et al. Spatially and size selective synthesis of Fe-based nanoparticles on ordered mesoporous supports as highly active and stable catalysts for ammonia decomposition. Journal of the American Chemical Society. 2010; 132(40): 14152–14162.
75. Simonsen SB, Chakraborty C, Chorkendorff I, et al. Alloyed Ni-Fe nanoparticles as catalysts for NH_3 decomposition. Applied Catalysis A: General. 2012; 447: 22–31.
76. Zhang J, Müller JO, Zheng W, et al. Individual Fe−Co alloy nanoparticles on carbon nanotubes: structural and catalytic properties. Nano Letters. 2008; 8(9): 2738–2743.
77. Duan X, Qian G, Zhou X, et al. MCM-41 supported CoMo bimetallic catalysts for enhanced hydrogen production by ammonia decomposition. Chemical Engineering Journal. 2012; 207: 103–108.
78. Choi JG. Ammonia decomposition over vanadium carbide catalysts. Journal of Catalysis. 1999; 182(1): 104–116.
79. Zheng W, Cotter TP, Kaghazchi P, et al. Experimental and theoretical investigation of molybdenum carbide and nitride as catalysts for ammonia decomposition. Journal of the American Chemical Society. 2013; 135(9): 3458–3464.
80. Guo J, Wang P, Wu G, et al. Lithium imide synergy with 3d transition-metal nitrides leading to unprecedented catalytic activities for ammonia decomposition. Angewandte Chemie. 2015; 127(10): 2993–2997.
81. Ogasawara K, Nakao T, Kishida K, et al. Ammonia decomposition over CaNH-supported Ni catalysts via an NH_2–vacancy-mediated Mars–van Krevelen mechanism. ACS Catalysis. 2021; 11(17): 11005–11015.
82. Chen C, Wu K, Ren H, et al. Ru-based catalysts for ammonia decomposition: a mini-review. Energy & Fuels. 2021; 35(15): 11693–11706.
83. Afonso RV, Gouveia JD, Gomes JR. Catalytic reactions for H_2 production on multimetallic surfaces: a review. Journal of Physics: Energy. 2021; 3(3): 032016.
84. Hirscher M, Yartys VA, Baricco M, et al. Materials for hydrogen-based energy storage–past, recent progress and future outlook. Journal of Alloys and Compounds. 2020; 827: 153548.

85. García-Bordejé E, Armenise S, Roldán L. Toward practical application of H_2 generation from ammonia decomposition guided by rational catalyst design. Catalysis Reviews. 2014; 56(2): 220–237.
86. Hosono H, Kitano M. Advances in materials and applications of inorganic electrides. Chemical Reviews. 2021; 121(5): 3121–3185.
87. Hosono H. Field-assisted green ammonia synthesis. Science Bulletin. 2024; 69(1): 7–8.
88. Aika K, Christiansen LJ, Dybkjaer I, et al. Ammonia: Catalysis and Manufacture. Springer; 2011.
89. Cao H, Guo J, Chand F, et al. Transition and alkali metal complex ternary amides for ammonia synthesis and decomposition. Chemistry—A European Journal. 2017; 23(41): 9766–9771.
90. Guo J, Chen P. Interplay of alkali, transition metals, nitrogen, and hydrogen in ammonia synthesis and decomposition reactions. Accounts of Chemical Research. 2021; 54(10): 2434–2444.
91. Gao W, Wang P, Guo J, et al. Barium hydride-mediated nitrogen transfer and hydrogenation for ammonia synthesis: a case study of cobalt. ACS Catalysis. 2017; 7(5): 3654–3661.
92. Wang P, Xie H, Guo J, et al. The formation of surface lithium–iron ternary hydride and its function on catalytic ammonia synthesis at low temperatures. Angewandte Chemie. 2017; 129(30): 8842–8846.
93. Luo Z, Castleman AW, Khanna SN. Reactivity of metal clusters. Chemical Reviews. 2016; 116(23): 14456–14492.
94. Cui C, Jia Y, Zhang H, et al. Plasma-Assisted Chain Reactions of Rh_3^+ Clusters with Dinitrogen: N≡ N Bond Dissociation. The Journal of Physical Chemistry Letters. 2020; 11(19): 8222–8230.
95. Saitoh H, Takagi S, Matsuo M, et al. Li_4FeH_6: Iron-containing complex hydride with high gravimetric hydrogen density. APL Materials. 2014; 2(7): 076103.
96. Yvon K, Renaudin G. Hydrides: solid state transition metal complexes. In: Encyclopedia of Inorganic Chemistry. Wiley; 2006.
97. Wang Q, Pan J, Guo J, et al. Ternary ruthenium complex hydrides for ammonia synthesis. ChemRxiv preprint. 2020. doi: 10.26434/chemrxiv.13465760.v1
98. Strongin D, Carrazza J, Bare SR, et al. The importance of C_7 sites and surface roughness in the ammonia synthesis reaction over iron. Journal of Catalysis. 1987; 103(1): 213–215.
99. Dahl S, Logadottir A, Egeberg RC, et al. Role of steps in N_2 activation on Ru (0001). Physical Review Letters. 1999; 83(9): 1814–1817.
100. Fukui K, Iimura S, Iskandarov A, et al. Room-temperature fast H–conduction in oxygen-substituted lanthanum hydride. Journal of the American Chemical Society. 2022; 144(4): 1523–1527.
101. Jiang Y, Takashima R, Nakao T, et al. Boosted Activity of Cobalt Catalysts for Ammonia Synthesis with $BaAl_2O_{4-x}H_y$ Electrides. Journal of the American Chemical Society. 2023; 145(19): 10669–10680.
102. Zhang Z, Miyashita K, Wu T, et al. Anion vacancies activate N_2 to ammonia on Ba–Si orthosilicate oxynitride-hydride. Nature Chemistry. 2025: 1–9.
103. Doyle W, Ingram D, Smith M. Detection of colloidal centers in lithium hydride by electron resonance. Physical Review Letters. 1959; 2(12): 497.
104. Cornelius S, Colombi G, Nafezarefi F, et al. Oxyhydride nature of rare-earth-based photochromic thin films. The Journal of Physical Chemistry Letters. 2019; 10(6): 1342–1348.
105. Cheng Z, Guan Y, Wen H, et al. Light-driven de/rehydrogenation of a LiH surface under ambient conditions. The Journal of Physical Chemistry Letters. 2024; 15(25): 6662–6667.
106. Guan Y, Wen H, Cui K, et al. Light-driven ammonia synthesis under mild conditions using lithium hydride. Nature Chemistry. 2024; 16(3): 373–379.
107. Feng S, Gao W, Cao H, et al. Advances in the chemical looping ammonia synthesis. Acta Chimica Sinica. 2020; 78(9): 916.
108. Zhang X, Pei C, Zhao ZJ, et al. Towards green and efficient chemical looping ammonia synthesis: design principles and advanced redox catalysts. Energy & Environmental Science. 2024; 17(7): 2381–2405.
109. Gálvez M, Halmann M, Steinfeld A. Ammonia production via a two-step Al_2O_3/AlN thermochemical cycle. 1. Thermodynamic, environmental, and economic analyses. Industrial & Engineering Chemistry Research. 2007; 46(7): 2042–2046.
110. Michalsky R, Pfromm PH. Chromium as reactant for solar thermochemical synthesis of ammonia from steam, nitrogen, and biomass at atmospheric pressure. Solar Energy. 2011; 85(11): 2642–2654.
111. Michalsky R, Pfromm PH. Thermodynamics of metal reactants for ammonia synthesis from steam, nitrogen and biomass at atmospheric pressure. AIChE Journal. 2012; 58(10): 3203–3213.
112. Michalsky R, Steinfeld A. Computational screening of perovskite redox materials for solar thermochemical ammonia

synthesis from N_2 and H_2O. Catalysis Today. 2017; 286: 124–130.
113. Moon J, Cheng Y, Daemen LL, et al. On the structural transformation of Ni/BaH_2 during a N_2-H_2 chemical looping process for ammonia synthesis: a joint in situ inelastic neutron scattering and first-principles simulation study. Topics in Catalysis. 2021; 64(9): 685–692.
114. Ravi M, Makepeace JW. Lithium–nitrogen–hydrogen systems for ammonia synthesis: exploring a more efficient pathway using lithium nitride–hydride. Chemical Communications. 2022; 58(41): 6076–6079.
115. Tang Z, Meng X, Shi Y, et al. Lithium-based loop for ambient-pressure ammonia synthesis in a liquid alloy-salt catalytic system. ChemSusChem. 2021; 14(21): 4697–4707.
116. Wang R, Gao W, Feng S, et al. Zn Promotes chemical looping ammonia synthesis mediated by LiH−Li_2NH couple. ChemSusChem. 2023; 16(22): e202300813.
117. Feng S, Gao W, Guo, J, et al. Electrodriven chemical looping ammonia synthesis mediated by lithium imide. ACS Energy Letters. 2023; 8(3): 1567–1574.
118. Wu H, Yang L, Wen J, et al. Plasma-driven nitrogen fixation on sodium hydride. Advanced Energy Materials. 2023; 13(27): 2300722.
119. Cui K, Guan Y, Cai Y, et al. Perovskite LiBaH3 for photo-assisted dinitrogen fixation. Science China Chemistry. 2025; 68(3): 1169–1174.
120. Yan H, Gao W, Wang Q, et al. Lithium palladium hydride promotes chemical looping ammonia synthesis mediated by lithium imide and hydride. The Journal of Physical Chemistry C. 2021; 125(12): 6716–6722.
121. Makepeace JW, Brittain JM, Manghnani AS, et al. Compositional flexibility in Li–N–H materials: implications for ammonia catalysis and hydrogen storage. Physical Chemistry Chemical Physics. 2021; 23(28): 15091–15100.
122. Tagawa K, Gi H, Shinzato K, et al. Improvement of kinetics of ammonia synthesis at ambient pressure by the chemical looping process of lithium hydride. The Journal of Physical Chemistry C. 2022; 126(5): 2403–2409.
123. Guan Y, Liu C, Wang Q, et al. Transition-metal-free barium hydride mediates dinitrogen fixation and ammonia synthesis. Angewandte Chemie International Edition. 2022; 61(39): e202205805.
124. Lim D, Kim A, Cheon S, et al. Life cycle techno-economic and carbon footprint analysis of H_2 production via NH_3 decomposition: A Case study for the Republic of Korea. Energy Conversion and Management. 2021; 250: 114881.
125. Jiao F, Xu B. Electrochemical ammonia synthesis and ammonia fuel cells. Advanced Materials. 2019; 31(31): 1805173.
126. Ramalingam S, DhakshinaMoorthy M, Subramanian S. Effect of natural antioxidant additive on hydrogen-enriched biodiesel operated compression ignition engine. International Journal of Hydrogen Energy. 2022; 47(48): 20771–20783.
127. Giddey S, Badwal S, Kulkarni A. Review of electrochemical ammonia production technologies and materials. International Journal of Hydrogen Energy. 2013; 38(34): 14576–14594.
128. Bell TE, Torrente-Murciano L. H_2 production via ammonia decomposition using non-noble metal catalysts: A review. Topics in Catalysis. 2016; 59: 1438–1457.
129. Cechetto V, Di Felice L, Medrano JA, et al. H_2 production via ammonia decomposition in a catalytic membrane reactor. Fuel Processing Technology. 2021; 216: 106772.
130. Pashchenko D, Mustafin R. Ammonia decomposition in the thermochemical waste-heat recuperation systems: A view from low and high heating value. Energy Conversion and Management. 2022; 251: 114959.
131. Ju X, Liu L, Yu P, et al. Mesoporous Ru/MgO prepared by a deposition-precipitation method as highly active catalyst for producing CO_x-free hydrogen from ammonia decomposition. Applied Catalysis B: Environmental. 2017; 211: 167–175.
132. Wang S, Yin S, Li L, et al. Investigation on modification of Ru/CNTs catalyst for the generation of CO_x-free hydrogen from ammonia. Applied Catalysis B: Environmental. 2004; 52(4): 287–299.
133. Moszczyńska J, Liu X, Wiśniewski M. Green hydrogen production through ammonia decomposition using non-thermal plasma. International Journal of Molecular Sciences. 2023; 24(18): 14397.
134. Lucentini I, Garcia X, Vendrell X, et al. Review of the decomposition of ammonia to generate hydrogen. Industrial & Engineering Chemistry Research. 2021; 60(51): 18560–18611.
135. Verschoor JC, de Jongh PE, Ngene P. Recent advances in thermocatalytic ammonia synthesis and decomposition. Current Opinion in Green and Sustainable Chemistry. 2024; 50: 100965.
136. Turaeva N, Fushimi R, Yablonsky G. Kinetic expression for optimal catalyst electronic configuration: The case of ammonia decomposition. The Journal of Physical Chemistry C. 2020; 124(48): 26310–26319.
137. Yang M, Raucci U, Parrinello M. Reactant-induced dynamics of lithium imide surfaces during the ammonia

decomposition process. Nature Catalysis. 2023; 6(9): 829–836.
138. Chen P, Zhu M. Recent progress in hydrogen storage. Materials Today. 2008; 11(12): 36–43.
139. Titherley AW. XLV.—Sodium, potassium, and lithium amides. Journal of the Chemical Society, Transactions. 1894; 65: 504–522.
140. Chen P, Xiong Z, Luo J, et al. Interaction between lithium amide and lithium hydride. The Journal of Physical Chemistry B. 2003; 107(39): 10967–10970.
141. Gao W, Guo J, Chen P. Hydrides, amides and imides mediated ammonia synthesis and decomposition. Chinese Journal of Chemistry. 2019; 37(5): 442–451.
142. David WI, Makepeace JW, Callear SK, et al. Hydrogen production from ammonia using sodium amide. Journal of the American Chemical Society. 2014; 136(38): 13082–13085.
143. Guo J, Chang F, Wang P, et al. Highly Active MnN–Li_2NH Composite Catalyst for Producing COx-Free Hydrogen. ACS Catalysis. 2015; 5(5): 2708–2713.
144. Medford AJ, Vojvodic A, Hummelshøj JS, et al. From the Sabatier principle to a predictive theory of transition-metal heterogeneous catalysis. Journal of Catalysis. 2015; 328: 36–42.
145. Mambretti F, Raucci U, Yang M, et al. How does structural disorder impact heterogeneous catalysts? The case of ammonia decomposition on non-stoichiometric lithium imide. ACS Catalysis. 2024; 14(3): 1252–1256.
146. Yu P, Guo J, Liu L, et al. Ammonia decomposition with manganese nitride–calcium imide composites as efficient catalysts. ChemSusChem. 2016; 9(4): 364–369.
147. Chang F, Guo J, Wu G, et al. Influence of alkali metal amides on the catalytic activity of manganese nitride for ammonia decomposition. Catalysis Today. 2017; 286: 141–146.
148. Chang F, Wu H, van der Pluijm R, et al. Effect of pore confinement of $NaNH_2$ and KNH_2 on hydrogen generation from ammonia. The Journal of Physical Chemistry C. 2019; 123(35): 21487–21496.
149. Guo J, Chen Z, Wu A, et al. Electronic promoter or reacting species? The role of $LiNH_2$ on Ru in catalyzing NH3 decomposition. Chemical Communications. 2015; 51(82): 15161–15164.
150. Kishida K, Kitano M, Inoue Y, et al. Large oblate hemispheroidal ruthenium particles supported on calcium amide as efficient catalysts for ammonia decomposition. Chemistry—A European Journal. 2018; 24(31): 7976–7984.
151. Chiuta S, Everson RC, Neomagus HW, et al. Reactor technology options for distributed hydrogen generation via ammonia decomposition: A review. International Journal of Hydrogen Energy. 2013; 38(35): 14968–14991.
152. Bergstrom F, Fernelius WC. The Chemistry of the Alkali Amides. Chemical Reviews. 1933; 12(1): 43–179.
153. Kojima Y, Miyaoka H, Ichikawa T. Hydrogen Storage Materials. In: New and Future Developments in Catalysis. Elsevier; 2013. pp. 99–136.
154. Leng H, Ichikawa T, Hino S, et al. Synthesis and decomposition reactions of metal amides in metal–N–H hydrogen storage system. Journal of Power Sources. 2006; 156(2): 166–170.
155. Leng H, Ichikawa T, Isobe S, et al. Desorption behaviours from metal–N–H systems synthesized by ball milling. Journal of Alloys and Compounds. 2005; 404: 443–447.
156. Zhang T, Isobe S, Wang Y, et al. A solid–solid reaction enhanced by an inhomogeneous catalyst in the (de) hydrogenation of a lithium–hydrogen–nitrogen system. RSC Advances. 2013; 3(18): 6311–6314.
157. Sudik A, Yang J, Halliday D, et al. Kinetic improvement in the Mg $(NH_2)_2$− LiH storage system by product seeding. The Journal of Physical Chemistry C. 2007; 111(17): 6568–6573.
158. Yin SF, Xu BQ, Wang SJ, et al. Magnesia–carbon nanotubes (MgO–CNTs) nanocomposite: Novel support of Ru catalyst for the generation of CO x-free hydrogen from ammonia. Catalysis Letters. 2004; 96: 113–116.
159. Raróg-Pilecka W, Szmigiel D, Kowalczyk Z, et al. Ammonia decomposition over the carbon-based ruthenium catalyst promoted with barium or cesium. Journal of Catalysis. 2003; 218(2): 465–469.
160. Sørensen RZ, Nielsen LJE, Jensen S, et al. Catalytic ammonia decomposition: miniaturized production of COx-free hydrogen for fuel cells. Catalysis Communications. 2005; 6(3): 229–232.
161. Klerke A, Klitgaard SK, Fehrmann R. Catalytic ammonia decomposition over ruthenium nanoparticles supported on nano-titanates. Catalysis Letters. 2009; 130: 541–546.
162. Hull S, Smith RI, David WI, et al. The Polaris powder diffractometer at ISIS. Physica B: Condensed Matter. 1992; 180: 1000–1002.
163. Dong X, Zhu S, Li H. Recent research progress of catalysts for thermocatalytic ammonia decomposition. International Journal of Hydrogen Energy. 2025; 143: 286–306.
164. Feng S, Gao W, Wang R, et al. Chemical looping ammonia decomposition mediated by alkali metal and amide pairs for H_2 production and thermal energy storage. Advanced Energy Materials. 2024; 14(43): 2401252.